

# SEA: Shareable and Explainable Attribution for Query-based Black-box Attacks

Yue Gao<sup>1</sup>, Ilia Shumailov<sup>2</sup>, Kassem Fawaz<sup>1</sup>

<sup>1</sup>University of Wisconsin–Madison, <sup>2</sup>University of Oxford

## Abstract

Machine Learning (ML) systems are vulnerable to adversarial examples, particularly those from query-based black-box attacks. Despite various efforts to detect and prevent such attacks, there is a need for a more comprehensive approach to logging, analyzing, and sharing evidence of attacks. While classic security benefits from well-established forensics and intelligence sharing, Machine Learning is yet to find a way to profile its attackers and share information about them. In response, this paper introduces SEA, a novel ML security system to characterize black-box attacks on ML systems for forensic purposes and to facilitate human-explainable intelligence sharing. SEA leverages the Hidden Markov Models framework to attribute the observed query sequence to known attacks. It thus understands the attack’s progression rather than just focusing on the final adversarial examples. Our evaluations reveal that SEA is effective at attack attribution, even on their second occurrence, and is robust to adaptive strategies designed to evade forensics analysis. Interestingly, SEA’s explanations of the attack behavior allow us even to fingerprint specific minor implementation bugs in attack libraries. For example, we discover that the SignOPT and Square attacks implementation in ART v1.14 sends over 50% specific zero difference queries. We thoroughly evaluate SEA on a variety of settings and demonstrate that it can recognize the same attack’s second occurrence with 90+% Top-1 and 95+% Top-3 accuracy.

## 1 Introduction

Machine learning (ML) systems are vulnerable to adversarial examples, where imperceptible perturbations to the input data can change its prediction [9,61]. Among the existing attacks, query-based black-box attacks are particularly concerning in practice. To generate an adversarial example, they only need to interact with the model through a sequence of queries without any knowledge of its architecture or gradients [7,13,19,54]. Despite substantial efforts to detect [17,39] and prevent [11,16,50] such attacks, logging, analyzing, and sharing the full evidence of the attack remains under-explored.

Traditional security relies on *forensics*, i.e., retrospective analysis of incidents to aid future detection and recovery [26,36,69], and *intelligence sharing*, i.e., the dissemination of critical incident details to impede future attack success in different contexts [4,56]. While traditional security benefits from well-established techniques like public CVE trackers [1], CERT systems [3], and open attack frameworks like Metasploit, the study of forensics and intelligence sharing is limited in Machine Learning.

Existing research primarily focuses on the adversarial attribution problem [33], which seeks to understand the hidden signatures in adversarial examples, often in the context of less concerning white-box attacks [12,42]. These works model the attribution problem as a deep learning classification task, attempting to extract all information of the attacker from a single adversarial example [24,33,43,45]. However, this approach requires vast amounts of adversarial examples, meaning that the same attack must happen thousands of times before it can be characterized and identified. Furthermore, these studies overlook a critical

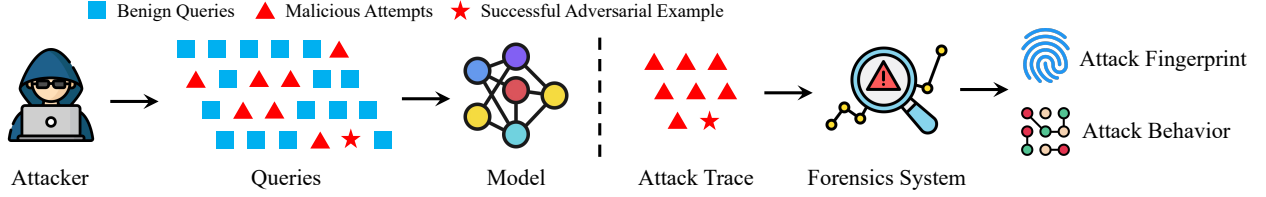


Figure 1: The general scenario for our forensics system. **Left:** The attacker sends malicious queries to the model to construct an adversarial example. **Right:** After the attack has triggered a security alarm, the forensics system extracts the attack’s trace to attribute, explain, and share the attack’s behavior.

aspect of forensics analysis, namely, that attribution outcomes must be shareable and explainable. The need to distribute deep learning models and signatures for knowledge sharing is neither practical nor efficient.

In this paper, we introduce SEA, a novel ML security system designed to analyze black-box attacks against ML systems for forensic purposes and enable human-explainable intelligence sharing. SEA can characterize an attack on its *first* occurrence and accurately recognize subsequent occurrences of the same attack. More importantly, the attribution it provides is understandable by humans.

Achieving these objectives presents several challenges. First, black-box attacks often employ a wide range of strategies to probe the adversarial space due to their query-only access. This makes it harder to characterize them within a unified framework. Second, characterizing an attack on its first occurrence demands data efficiency, which is hard to solve given a single adversarial example. Third, deep learning-based methods explored by existing research lack explainability and are not easily shareable.

We tackle these challenges by examining the progression of an attack, i.e., the sequence of queries extracted from logged history queries, rather than merely the final adversarial example. By analyzing the attack’s progression, we can describe its behavior at a finer granularity, as the most meaningful information of an attack is embedded within its query sequence. Building upon this intuition, we model black-box attacks using a unified framework based on Hidden Markov Models. This model allows the analyst to attribute the observed query sequence to internal attack procedures. Leveraging the well-established theoretical framework of HMMs, SEA achieves data-efficient, explainable, and shareable attack fingerprints. Figure 1 illustrates its pipeline.

We thoroughly evaluate SEA and demonstrate its ability to characterize and identify a variety of state-of-the-art attacks. In particular, we show that:

- SEA can characterize an attack’s behavior on its *first* occurrence and produce a fingerprint immediately. The fingerprint is a small easy-to-share matrix that describes the attack’s overall behavior.
- SEA can recognize the same attack’s *second* occurrence with 90+% Top-1 and 95+% Top-3 accuracy on multiple datasets and models. The performance improves further when more fingerprints of that attack are available.
- SEA can explain the attack’s behavior at a per-query granularity. This explainability leads us to discover specific implementation bugs in attack libraries. For example, we discover that the `SignOPT` [19] and `Square` [7] attacks implementation in the ART library (v1.14) [46] sends over 50% duplicated queries, making it easy to distinguish from other libraries.
- SEA is robust to several adaptive attacks that aim to evade forensics analysis. While employing adaptive strategies changes the nature of the attack on their first occurrence, SEA can treat them as different attacks and eventually recognize such strategies with high accuracy.

## 2 Background and Related Work

In this section, we introduce the background and related work on black-box adversarial examples and forensics.

### 2.1 Black-box Adversarial Examples

Given a clean input  $\mathbf{x} \in \mathbb{D} := [0, 1]^d$  and a classifier  $f$ , the adversarial example  $\mathbf{x}'$  is visually similar to  $\mathbf{x}$  but misclassified, i.e.,  $f(\mathbf{x}') \neq f(\mathbf{x})$  [9, 61]. Typical attacks achieve visual similarity by bounding the perturbation by a budget  $\epsilon$  in  $\ell_p$  norm, where  $\|\mathbf{x} - \mathbf{x}'\|_p \leq \epsilon$ . We use boldface to denote vectors in this paper (e.g.,  $\mathbf{x}$ ).

#### 2.1.1 Black-box Attacks

A black-box attack  $\mathcal{A}$  only has query access to the classifier and possesses no knowledge of the classifier’s architecture or gradients. To generate an adversarial example  $\mathbf{x}'$ , the attack can only interact with the classifier through a sequence of  $n$  queries  $X = \{\mathbf{x}_t\}_{t=1}^n$ , where  $\mathbf{x}_n$  is the final adversarial example. We refer to this query sequence as the *attack’s trace*.

Existing query-based black-box attacks can be categorized into *score-based* and *decision-based* attacks based on their assumptions of the classifier’s outputs. Score-based attacks assume the classifier returns the confidence score for each query, which facilitates estimation of the classifier’s gradients [7, 15, 31, 34, 44]. Decision-based attacks assume the classifier returns only the predicted label. In this challenging yet more practical setting, the attacks usually walk near the decision boundary [10, 13, 14, 38, 54] to find the minimally perturbed adversarial example or optimize for a particular objective function [18, 19, 40].

With additional assumptions of the classifier’s architecture or data distribution, query-free black-box attacks can avoid repeatedly querying the model by leveraging the transferability of adversarial examples [49]. Such attacks train a substitute model approximating the victim classifier’s decision boundary and mainly attempt to improve transferability [23, 66, 68]. Detailed analysis of query-free attacks remains challenging as they can be reduced to the white-box threat model [12, 42] with full access to the classifier’s architecture and gradients.

In this paper, we cover a wide range of recent attacks:

- *Score-based*: Square [7], ECO [44], NES [34].
- *Decision-based*: HSJ [13], GeoDA [54], SignOPT [19], Boundary [10], RayS [14].

We also include the  $\ell_2$  and  $\ell_\infty$  variants of each attack if it supports and adopts different strategies, totaling 11 distinct attack variants. We explain their details in Appendix B.2.

#### 2.1.2 Black-box Defenses

Defenses against black-box attacks fall into three broad categories: detection-based, pre-processing, and post-processing defenses.

Detection defenses identify queries generated by black-box attacks and reject or return incorrect outputs. SD [17] inspects each query’s mean pair-wise distance to each account’s history queries. PRADA [35] inspects the query’s distributional shifts among different accounts; it was originally designed for model stealing attacks [63] but is effective for evasion attacks [17]. Blacklight [39] detects overly similar queries

in the input space. It introduces a compact hash function that is sensitive to small changes in the image using a segment-based probabilistic fingerprint.

Pre-processing defenses [32, 47, 53, 67] aim to increase the cost of finding adversarial examples with randomized input transformations. While their efficacy in the white-box setting is limited both empirically [8, 58, 62] and theoretically [30], they remain effective in the black-box setting [5, 11, 50]. Post-processing defenses modify the model outputs to interfere with the attack [16, 48].

Our forensics system **SEA is complementary to the above defenses**. For example, upon receiving a report about an active black-box attack, instead of blocking the attack immediately, the defender can allow the attack to proceed. Then, our system would analyze the attack’s behavior.

## 2.2 Digital Forensics

Forensic techniques offer a complementary approach for investigating an attack after it has occurred. They can uncover valuable information about the attacker, such as their identity and unique behaviors.

### 2.2.1 Forensics Research in Machine Learning

Existing forensics research in machine learning primarily focuses on the Adversarial Attribution Problem (AAP) [33], which aims to understand the hidden signatures in adversarial examples, such as the attack algorithm and hyper-parameters [24, 33, 43, 45]. While our work tackles a similar problem, it offers significant contributions beyond existing work:

- **Explainability.** Prior works cannot provide explainability for their attribution results. Yet, explaining the attribution results is critical in forensics, as it helps human analysts understand and explain the attack’s behavior. A standalone attribution only provides limited information in practice. We leverage our modeling of black-box attacks to explain the attack’s behavior at the per-query granularity.
- **Sharing.** Prior works model the attribution problem as a deep-learning classification task. To share the knowledge of an attack, they have first to collect vast amounts of data (i.e., the same attack is observed thousands of times) and then distribute the deep learning model. This scenario is neither practical nor efficient. Our system fingerprints the attack on its first occurrence and can immediately recognize its subsequent occurrences with high accuracy.

In summary, while prior works mainly tackle the standalone attribution problem, we deliver a system that covers the several objectives in forensics, including attribution, explanation, and sharing.

### 2.2.2 Distinction from Black-box Defenses

As complementary approaches, forensics and defenses share aspects of the threat model: the attacker aims to compromise the system, and the victim aims to prevent or investigate the attack. However, there is a critical distinction in their threat models that provide an advantage to the forensics system.

The adversarial machine learning literature has shown that designing robust defenses against adversarial examples is challenging both empirically and theoretically [8, 30, 62]. The root cause of this problem, like other security problems, is that the attack can always adapt its technique to the deployed defense until a successful circumvention [62].

However, when it comes to forensics, although the attack can still adapt its strategy [22, 59, 60], it is the forensics system that makes the ultimate adaptation [57]. As long as the attack has finished and left a trace

(which cannot be changed later), the forensics system can keep adapting its techniques until a successful investigation. Defenses do not have such chances to adapt after the attack has succeeded. Moreover, actively adapting to a forensics system usually comes with a higher query or budget cost, or requires a full system compromise to alter the append-only logs.

### 3 Evasion Forensics

In this paper, we consider forensics analysis of query-based black-box attacks on classifiers. Given a reported adversarial example, we aim to identify the associated query trace and attribute it to the most probable underlying attack. Figure 1 illustrates the general outline of this task.

#### 3.1 Threat Model

We first describe our threat model, followed by the attacker assumptions. Finally, we cover SEA forensic system.

##### 3.1.1 Attacker

We focus on the standard threat model of query-based black-box attacks, where the attacker issues a sequence of  $n$  queries  $X = \{\mathbf{x}_t\}_{t=1}^n$  to the model to generate an adversarial example,  $\mathbf{x}' = \mathbf{x}_n$ . We refer to this query sequence as the attack’s trace. The model returns the final predicted label, potentially with a confidence score. The attacker does not have any knowledge of the classifier’s architecture or gradients. We also assume that the final adversarial example is bounded by a perturbation budget  $\epsilon$  under some distance metric, such as the  $\ell_p$  norm distance.

##### 3.1.2 Forensics System

We assume SEA is deployed by the Model-as-a-Service (MaaS) platform to identify which attack generated an adversarial example  $\mathbf{x}'$ . SEA has access to the adversarial example as well as the history queries  $Q$ , which contain the attack’s trace  $X \subseteq Q$ . SEA assumes access to history queries because forensic analysis is only possible with access to the attack’s trace, implying an inevitable storage cost. We thus consider scenarios where security objectives outweigh the storage cost. In Section 7.4.2, we study the trade-off between performance and storage.

In practice, SEA can work in tandem with black-box detection defenses, such as SD [17] and Blacklight [39]. Upon receiving a report about a black-box attack, instead of blocking the attack, the defender can allow the attack to proceed. Then, SEA would analyze the attack’s trace.

#### 3.2 Problem Definition

Given an adversarial example, SEA aims to attribute its attack trace to a known attack (if possible), provide the analyst with the rationale behind its attribution, and share attack knowledge with other parties. Specifically, SEA has the following three objectives:

1. **Sharing.** The system should produce a shareable fingerprint that concisely represents the underlying attack. This process would help link potentially related incidents to the observed attack. It is preferable to achieve sharing with high data efficiency: the system should ideally learn the fingerprint from the attack’s first occurrence (i.e., a single trace).

2. **Explanation.** The system should be able to explain its attribution results. A good explanation should generally describe the underlying attack’s behavior, or at least the factors that result in the attribution.
3. **Attribution.** The system should attribute a given trace to a known attack with high accuracy. The attribution should adapt to the attack’s behavior change, yet it should generalize to different datasets, models, and future invocations of the same attack.

### Theoretical Limitation

We acknowledge a theoretical limitation in the task we aim to solve, where pursuing a perfect solution could be intractable. SEA attempts to solve an instance of an inverse problem: observing a sequence of queries, it tries to find the attack that generated them. Such a problem is hard to solve as infinitely many programs can produce a given trace. Hence, it is difficult to provide a guarantee for generalization across datasets, models, and attack runs. Attributing the observed trace to some attack only allows us to argue that this attack is the most likely source among a set of known attacks.

### 3.3 Attack Identity

Attack *identity* is a key concept in the attribution task. Given the above limitations, we define attack identity based on the attack’s observed outputs, instead of its exact algorithm or specifications. We model the attack attribution problem as an  $M$ -ary hypothesis testing problem, where each attack identity is a hypothesis and  $M$  is the number of attacks. Each attack identity  $\mathcal{A}_i$  is associated with a probability distribution  $\mathcal{P}_{\mathcal{A}_i}$ , with density  $P_{\mathcal{A}_i} = \Pr[X \mid \mathcal{A}_i]$ , over all possibly generated traces. We assume that all attacks happen with the same probability so that, given a trace  $X$ , the optimal decision rule is choosing the attack with the maximum likelihood  $P_{\mathcal{A}_i}(X)$ ; i.e.,  $\mathcal{A}^* = \arg \max_{i \in [M]} P_{\mathcal{A}_i}(X)$ .

With this definition, SEA chooses the optimal hypothesis for a given trace  $X$  in the Bayesian setting. As the space of traces is intractable, it is not feasible to determine the decision rule ahead of time. Instead, SEA computes the probabilities of each attack generating the observed trace on the fly, and determines the most probable attack. We show in the next section how we model the black-box attack as a Hidden Markov Model (HMM) to obtain  $P_{\mathcal{A}_i}(X)$ . The advantage of this approach, compared to neural networks, is that provides an explainable final decision. An analyst will have access to how SEA attributes the trace to an attack.

## 4 Characterizing Black-box Attacks

In this section, we introduce novel modeling of black-box attacks with HMMs. This modeling allows us to characterize the behavior of black-box attacks in a unified framework, encompassing the many attacks, approaches, and strategies proposed in the black-box attack literature.

### 4.1 Visualizing Behavior of Black-box Attacks

A key property of this system is to model the observed attack behavior in a human-explainable way. This allows an analyst to understand the progression of an attack by studying it one query at a time. Generally, the best-known methods for characterizing attacks focus on detecting similar queries, which is considered the main feature for defending against any black-box attack [17, 39]. However, this approach is attack-agnostic, meaning it cannot differentiate between various types of attacks. In the following, we begin with

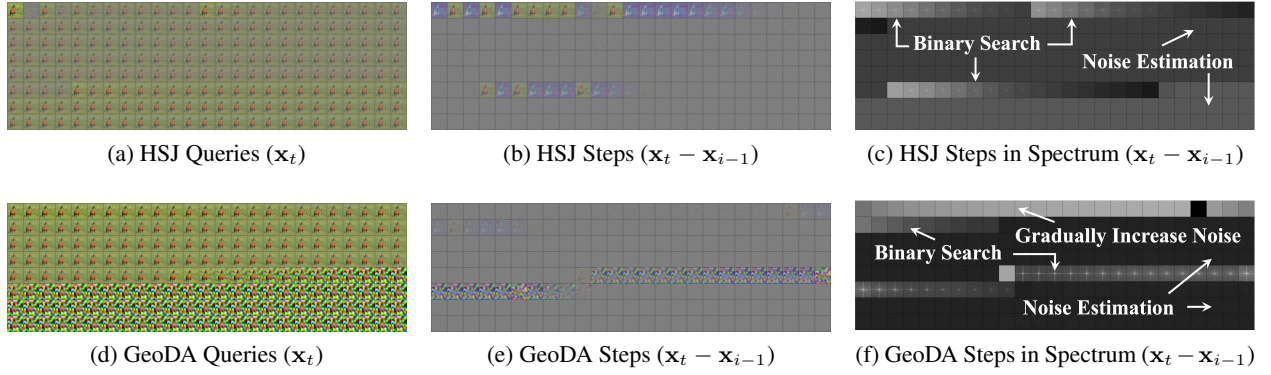


Figure 2: The first 200 queries of HSJ and GeoDA attacks. **Left:** It is hard to determine precisely what each attack is doing for each query. **Medium and Right:** Changes between successive queries demonstrate the precise human-identifiable behavior of two attacks, especially in the spectrum space.

a preliminary study to illustrate how attacks can be distinct, even when *human analysts* are observing their query sequences. Then, we build on this intuition to model black-box attacks with HMMs.

We first examine whether the raw queries from an attack can demonstrate a unique human-identifiable behavior. We visualize 200 queries of HSJ [13] and GeoDA [54] attacks against the same clean image in Figures 2a and 2d. Although there are some differences between the two attack traces, it is hard to identify precisely what each attack is doing for each query. In particular, it is not immediately clear to a human observer how to break down the trace into a fine-grained set of attack phases.

We then examine the per-query *changes* between successive queries  $\delta_t = \mathbf{x}_t - \mathbf{x}_{t-1}$  and visualize them in Figures 2b and 2e. At this point, we can clearly observe the fine-grained behaviors of the two attacks. For example, we can easily identify the different attack phases of line search, gradient estimation, and the different spectrum patterns of their estimated gradients. It is worth noting that the above changes only visualize the attack’s observed behavior instead of its design. For example, decision-based black-box attacks might send independent noise samples to estimate gradients without incrementally changing the query at each time step [13, 18, 54]. However, because these queries are sequential, the observed changes between them can still characterize the attack’s effective behavior.

The visualization in Figure 2 shows that it is possible to apply forensics analysis to the trace of black-box attacks. While this visual interpretation can already help a forensic analyst identify and explain the behavior of different attacks, it amounts to an intuitive understanding that is hard to formalize and, more importantly, share to different parties. We still need a systematic and quantitative framework to characterize these behaviors.

## 4.2 Modeling Black-box Attacks as HMMs

A common description of black-box attacks is that they are programs that repeatedly query the model [21]. Prior research established that decision-based black-box attacks usually consist of a fixed set of procedures, such as gradient estimation and line search [29], and such procedures can be decomposed further into scalar and vector operations [28]. However, an external party (e.g., the victim model) has no way to observe the internal state of the attack, including which internal procedures are executed. When observing the query trace, the best the victim can do is to attribute the observed behavior to different internal procedures over

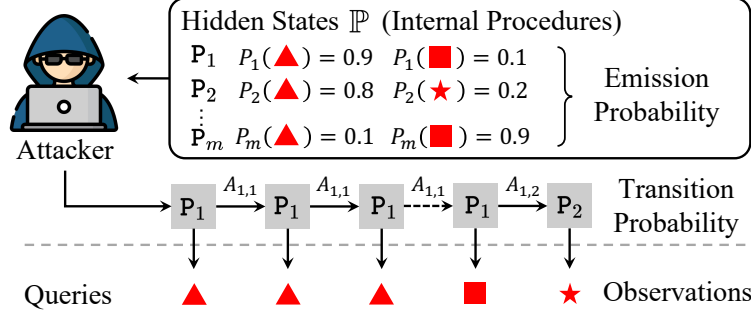


Figure 3: Illustration of our HMM modeling of black-box attacks.

time. *This scenario is exactly what Hidden Markov Models (HMMs) aim to characterize.*

Specifically, an HMM consists of a sequence of *hidden states* and *observations*. Hidden states represent an underlying system that evolves over time but cannot be directly observed, while observations are the measurable outcomes of such hidden states. One of the key objectives of HMMs is to understand the hidden states based on the observations and their probabilistic relationships.

Therefore, we can easily notice an analogy between the black-box attack and the HMM, as illustrated in Figure 3. From an external party’s perspective, the black-box attack can be viewed as a stochastic process — at each step, the attack randomly chooses an internal *procedure*, which randomly produces a *query*. One may argue that black-box attacks are deterministic (given an input example, target model, and seed), but this is only the case when the underlying attack is known. For an unknown attack under analysis, its behavior can still be characterized by a stochastic process.

### Attack Model

Motivated by the above analogy, we propose to model black-box attacks as an HMM that consists of *procedures* and *queries*. In this setting, we are able to unify black-box attacks under the HMM’s theoretical framework, and leverage all its available theoretical tools. We now formalize a given black-box attack using the HMM notation:

- **Observations.** Each observation represents a query from the attack, so the space of observations is  $\mathbb{D} := [0, 1]^d$  as we have defined in Section 2.1. This space is discrete with size  $|\mathbb{D}| = 256^d$  due to image quantization.
- **Hidden States.** We denote the space of hidden states as  $\mathbb{P} := \{P_j\}_{j=1}^m$ , where each state  $P_j$  represents an internal procedure of attacks, and  $m$  is the total number of states.
- **Emission Probability.** Each state  $P_j$  has an emission probability distribution  $\mathcal{P}_j$  with PMF  $P_j(\mathbf{x}_t | \mathbf{x}_{t-1})$ , which defines the probability of state  $P_j$  producing a query  $\mathbf{x}_t$  given its previous query  $\mathbf{x}_{t-1}$ . The probability is conditional because we analyze the changes between queries.
- **Transition Probability.** The transition probability  $A \in [0, 1]^{m \times m}$  characterizes how each state transits to the next state, where  $A_{i,j} := \Pr[P^{(t)} = P_j | P^{(t-1)} = P_i]$  is the probability of choosing  $P_j$  given the previous state  $P_i$ .



## Attack Representation

Given the above formalization, we represent each attack as an HMM parameterized by  $\mathcal{A}_i = (A, \phi)$ , where the emission probability  $\phi := \{P_j\}_{j=1}^m$  is a global setting for all attacks, and  $A$  is the attack-specific transition matrix. This representation also instantiates the attack’s identity in Section 3.2; given the attack trace,  $X = \{\mathbf{x}_t\}_{t=1}^n$ , the probability  $P_{\mathcal{A}_i}(X)$  is

$$\begin{aligned} P_{\mathcal{A}_i}(X) &= \Pr[X \mid \mathcal{A}_i] = \sum_{j=1}^m \alpha_n(j), \\ \text{where } \alpha_{t+1}(j) &= \left[ \sum_{k=1}^m \alpha_t(k) \times A_{k,j} \right] \times P_j(\mathbf{x}_{t+1}) \\ \text{and } \alpha_1(j) &= \frac{1}{m} \times P_j(\mathbf{x}_1), \end{aligned} \tag{1}$$

where  $\alpha_t(k)$  is the forward probability of procedure  $\mathbb{P}_k$  at step  $t$ . This is known as the Forward algorithm [52].

## 4.3 Systemizing Black-box Attack Procedures

Finally, we define the procedures in our formalization of black-box attacks. By characterizing these attacks in a unified framework, we can systematize their procedures into two categories: *noise procedures* and *pattern procedures*. We define the probability distribution of each procedure  $\mathbb{P}$  as  $\mathcal{P}$  with the corresponding PMF  $P(\mathbf{x}_t \mid \mathbf{x}_{t-1})$ , which represents the probability of procedure  $\mathbb{P}$  producing a query  $\mathbf{x}_t$  given its previous query  $\mathbf{x}_{t-1}$ . We only model the abstract procedures here and defer their instantiations to Section 6.

We also note that it is impractical to model the ground-truth internal procedures of black-box attacks, i.e., conclusively predict the next query of an attack. *First*, modeling the internal procedure would require access to its source code, which is hard to assume for a novel attack in the wild. *Second*, the outputs of the internal procedure depend on the attack’s internal state and the target model responses, both of which can be random. In that case, the same procedure might exhibit different behaviors (hence hard to characterize). For example, the line search procedure generates almost empty changes as it converges. *Third*, using Monte Carlo simulations to estimate the probability distribution is not feasible as the output space is too large with  $|\mathbb{D}| = 256^d$ .

### 4.3.1 Noise Procedures

Noise procedures add noise to inputs, typically at the pixel level. Therefore, the changes  $\delta_t$  can be treated as i.i.d. noise at the pixel level. That is, for a given noise procedure and  $\mathbf{x}_t \sim \mathcal{P}$ , the pixels of its change  $\delta_t := \mathbf{x}_t - \mathbf{x}_{t-1}$  are independently drawn from an identical distribution  $\mathcal{P}'$ . We can thus define the PMF of  $\mathcal{P}$ , i.e., the emission probability in Section 4.2, as

$$P(\mathbf{x}_t \mid \mathbf{x}_{t-1}) := \Pr_{\delta_i \sim \mathcal{P}'} [\delta_1, \delta_2, \dots, \delta_d] = \prod_{i=1}^d \Pr_{\delta_i \sim \mathcal{P}'} [\delta_i], \tag{2}$$

where  $\{\delta_i\}_{i=1}^d$  are the pixel values of  $\delta_t$ .

The underlying pixel-level distribution  $\mathcal{P}'$  varies for different instances of noise procedures. We will explain how to discover and instantiate such procedures in Section 6.

### 4.3.2 Pattern Procedures

Pattern procedures lead to changes that exhibit correlation with a template. We define the PMF by matching the changes to observed patterns of procedures. Toward that end, we utilize a pattern matching metric  $\mathcal{M} : \mathbb{D} \rightarrow [0, 1]$  that measures the similarity between the change  $\delta_t$  and a given pattern  $\tau$ . Then, we transform the similarity score  $\mathcal{M}$  to a probability measure like what we have defined for noise procedures in Equation (2).

To compute the similarity score, we use the Pearson correlation coefficient, widely used in template matching:

$$\mathcal{M}(\delta_t, \tau) := |R(\delta_t, \tau)|, \quad (3)$$

where we ignore the sign because we are not interested in correlation direction, and  $R$  is given as:

$$R(\mathbf{z}_1, \mathbf{z}_2) = \frac{(\mathbf{z}_1 - \bar{\mathbf{z}}_1)(\mathbf{z}_2 - \bar{\mathbf{z}}_2)}{\|\mathbf{z}_1 - \bar{\mathbf{z}}_1\| \|\mathbf{z}_2 - \bar{\mathbf{z}}_2\|} \in [-1, 1]. \quad (4)$$

To transform this similarity score to a probability distribution, we enforce a truncated exponential distribution on  $\mathcal{M}$ :

$$P(\mathbf{x}_t | \mathbf{x}_{t-1}) := c \cdot \frac{1}{|\mathbb{D}|^{1-\mathcal{M}(\delta_t, \tau)}}, \quad (5)$$

where  $c$  is the normalization constant. This probability converges to one when the given change matches the pattern with a high score  $\mathcal{M}(\delta_t, \tau) = 1$ , and converges to zero as the score approaches zero. In Appendix A, we discuss the intuition of this transformation, as well as other definitions of  $\mathcal{M}$  that capture special patterns like linearity.

Similar to noise distributions, the underlying pattern  $\tau$  varies for different instances of pattern procedures. We will explain how to instantiate such patterns in Section 6.

### Summary

We have formalized black-box attacks under a unified framework with HMMs. In this framework, a black-box attack can be treated as a stochastic process, as illustrated in Figure 3. The transition probability between procedures can represent an attack’s behavior, hence its identity. We have also systematized two categories of procedures and defined their abstract probability distributions, which will be instantiated in Section 6.

## 5 System Design

In this section, we introduce the detailed design of our forensics system SEA. Given an adversarial example  $\mathbf{x}'$  and history queries  $Q$ , SEA executes the following workflow:

1. **Extract** attack trace from history queries (Section 5.1).
2. **Attribute** the attack’s observed behavior (Section 5.2).
3. **Share** the attack fingerprint (Section 5.3).

Eventually, SEA outputs a fingerprint for each attack that is shared and used for attribution. Figure 4 previews the generated fingerprints from SEA, which correspond to small transition matrices. To achieve its workflow, SEA builds and maintains the following resources:

- A **procedure database**  $\mathbb{P} = \{\mathcal{P}_i\}_{i=1}^m$ . Each procedure  $\mathcal{P}_i$  is represented by a probability distribution  $\mathcal{P}_i$  with PMF  $P_i(\mathbf{x})$ . This PMF defines the probability of state  $\mathcal{P}_i$  producing a given query  $\mathbf{x}$ .
- An **attack database**  $\mathbb{A} = \{\mathcal{A}_i\}_{i=1}^M$ . Each attack  $\mathcal{A}_i$  is represented by its transition matrix  $A \in \mathbb{R}^{m \times m}$ .
- SEA creates a **fingerprint database** to allow for sharing attacks, which will be explained in Section 5.3. In this database,  $\mathbb{F} = \{F_1, F_2, \dots\}$ , each fingerprint  $F_i$  is associated with an incident caused by some attack  $\mathcal{A}$ .

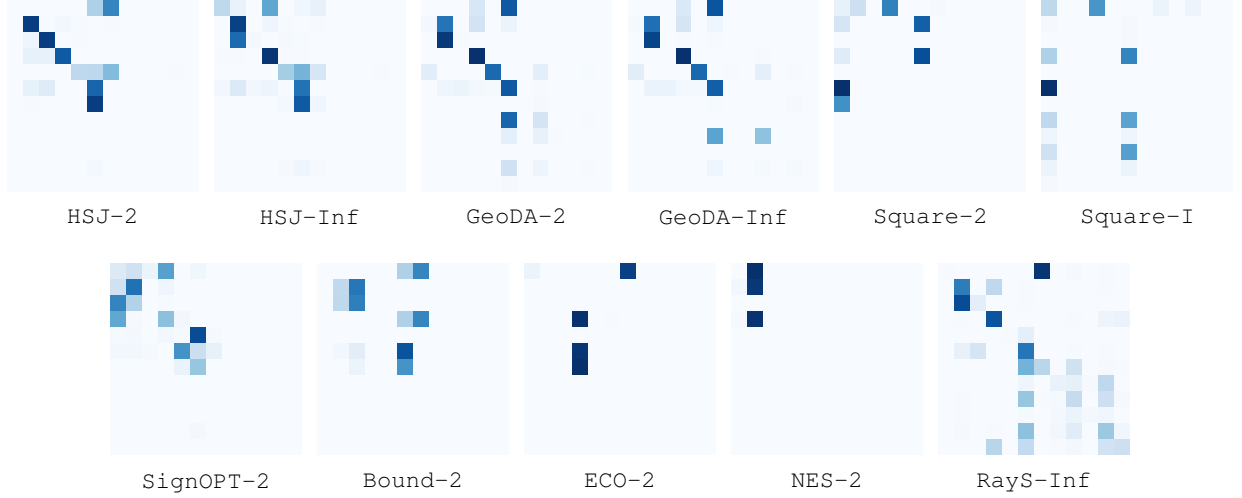


Figure 4: Illustration of the fingerprints of 11 attack variants we studied. Detailed numbers and confidence intervals can be found in Appendix B.4.

## 5.1 Extracting Attack Trace

The first step of SEA is to extract the attack trace  $X$  from history queries, where the last query  $\mathbf{x}_n$  is the given adversarial example  $\mathbf{x}'$ .

### 5.1.1 Theoretical Limitations

We first note that a perfect extraction of the attack trace is impossible. Although prior research has established that the queries from black-box attacks are very similar [17, 39], the attack may still produce heavily distorted queries that are uncorrelated with the final adversarial example. For example, decision-based attacks usually query the model with pure Gaussian noise to initialize their adversarial direction [13]. It is impossible to associate such queries with the underlying attack.

### 5.1.2 Identifying Similar Queries

Given the above limitations, we solve the extraction task by identifying history queries that are similar to the adversarial example  $\mathbf{x}'$ .

Identifying similar queries from black-box attacks is a challenging task for detection defenses, because they have to avoid the false-positive detection of benign similar queries like consecutive video frames.

However, a forensics system does not have such constraints because it has access to the given adversarial example — any query correlated with the adversarial example is arguably part of the attack trace.

As such, we extract the attack trace by clustering the queries that correlate with the given adversarial example. In particular, we employ DBSCAN [25] with the minimum points in a cluster equal to one and the distance metric being the correlation. The clustering starts with initializing the observed trace with the given adversarial example  $\mathbf{x}'$ . Then, SEA incrementally adds queries to the trace if there are history queries that exhibit a high correlation with at least one point in the trace:

```
Initialize:  $X := \{\mathbf{x}'\}$ 
Repeat:  $X \leftarrow X \cup \{\mathbf{x} \in Q \mid \exists \mathbf{z} \in X, R(\mathbf{z}, \mathbf{x}) \geq r\}.$ 
```

In the above,  $R$  is the correlation coefficient defined in Equation (4) and  $r$  is a system threshold. This threshold controls a trade-off between the completeness of the extracted trace and the inclusion of other benign queries. We evaluate this trade-off in Section 7.4.1. The widely-used value  $r = 0.5$  in template matching obtains the best performance.

## 5.2 Matching and Explaining Attack Patterns

After extracting the attack trace  $X$ , SEA can directly attribute this trace to a known attack and explain its pattern by leveraging the well-established HMM framework.

### 5.2.1 Matching Patterns

Attributing the observed trace to a known attack is equivalent to the problem of model selection in the context of HMMs. Given a set of HMMs, we want to determine which HMM mostly likely generates the sequence:

$$\mathcal{A}^* = \arg \max_{\mathcal{A} \in \mathbb{A}} \Pr[X \mid \mathcal{A}], \quad (6)$$

where  $\Pr[X \mid \mathcal{A}]$  is the probability of observing the sequence  $X$  given the HMM parameterized by  $\mathcal{A}$ . We omit other parameters like  $\mathbb{P}$  as they are shared by all HMMs. This problem can be solved by the Forward algorithm [52].

### 5.2.2 Explaining Patterns

Once we have determined the most likely attack  $\mathcal{A}^*$ , we can explain the attribution by inferring the most likely sequence of procedures behind the observed trace  $X$ . This is known as the decoding problem in the context of HMMs, which aims to find the most likely sequence of hidden states given the observed sequence:

$$Y^* = \arg \max_{Y \in \mathbb{P}^n} \Pr[Y \mid X, \mathcal{A}^*], \quad (7)$$

where  $\Pr[Y \mid X, \mathcal{A}^*]$  is the probability of procedure sequence  $Y = \{p^{(t)}\}_{t=1}^n$  given the trace  $X$  and the attack  $\mathcal{A}^*$ . This problem can be solved by the Viterbi algorithm [27], which computes the most likely sequence of hidden states.

### 5.3 Sharing Attack Fingerprints

Matching and explaining the attack trace only allows us to analyze the behavior of a local trace but not share such knowledge with other parties. SEA supports generating a fingerprint of the exact trace’s pattern, enabling a timely sharing of the observed attack incident. SEA uses the transition matrix,  $A$ , as the fingerprint of the observed attack trace. Over time, SEA would accumulate multiple fingerprints for each attack, each corresponding to an observed trace. Such a database of fingerprints would allow for attack attributions at multiple granularities, as will be discussed later.

Therefore, we need to find a transition matrix  $A$  that best describes an observed trace. This is known as the parameter estimation problem in HMMs:

$$\mathbf{F} := \hat{A} = \arg \max_{A \in \mathbb{R}^{m \times m}} \Pr[X | A]. \quad (8)$$

The estimated transition matrix  $\hat{A}$  is the fingerprint  $\mathbf{F}$  of the attack trace  $X$ . We obtain  $\hat{A}$  using the Expectation-Maximization algorithm [52], which finds the maximum likelihood estimate of  $\hat{A}$  given the observed data.

We can now attribute an observed trace to an attack or to an attack instance. Taking two fingerprints:  $\mathbf{F}_1$  from a previously observed attack instance and  $\mathbf{F}_2$  from a current trace, one can obtain their similarity by cosine similarity:

$$\text{cos-sim}(\mathbf{F}_1, \mathbf{F}_2) = \frac{\mathbf{F}_1 \cdot \mathbf{F}_2}{\|\mathbf{F}_1\| \|\mathbf{F}_2\|}, \quad (9)$$

where the fingerprints are flattened into vectors beforehand. It is also possible to attribute the observed trace by matching it to the attack with the most similar average fingerprint:

$$\mathcal{A}^* = \arg \max_{\mathcal{A} \in \mathbb{A}} \text{cos-sim} \left( \mathbf{F}, \sum_{\mathbf{F}' \in \mathbb{F}_{\mathcal{A}}} \frac{\mathbf{F}'}{|\mathbb{F}_{\mathcal{A}}|} \right), \quad (10)$$

where  $\mathbf{F}$  is the fingerprint being analyzed, and  $\mathbb{F}_{\mathcal{A}} \subseteq \mathbb{F}$  is the database of known fingerprints for attack  $\mathcal{A}$ . Being able to interpret and share fingerprints of attacks is another advantage of utilizing HMMs instead of neural networks for this task. Neural networks might provide superior performance but will lack explainability and shareability.

## 6 System Implementation

We now describe how we enrolled a set of known black-box attacks into SEA’s procedure database  $\mathbb{P}$  and the attack database  $\mathbb{A}$ . An analyst can use this process to enroll newly reported attacks to SEA. If the analyst has access to the source code of the attack, they can choose to define their set of procedures if not already covered. These can be noise procedures (Section 4.3.1), where the analyst defines the probability distribution of the noise, or pattern procedures (Section 4.3.2) where the analyst defines the template.

We also propose a semi-automated process to enroll attacks using a *single* observed trace. We used this process to implement SEA because it does not require access to the source code or multiple traces from the same attack. In the following, we describe this process, which involves (1) discovering unseen procedures from the attack trace, (2) estimating their probability distributions, and (3) including them in the database only if they significantly improve the existing estimations.

ID	Discovered From	Description
NULL	-	A query is identical to its previous one, caused by quantization or duplicated queries.
N1	HSJ-2	The difference between normalized standard Gaussian noise times a large constant.
N2	HSJ-2	The difference between normalized standard Gaussian noise times a small constant.
N3	GeoDA-2	The difference between non-normalized standard Gaussian noise.
N4	GeoDA-2	The difference between non-normalized standard Gaussian noise in the DCT subspace.
P1	GeoDA-2	A gradient update with horizontal and vertical spectral peaks.
P2	GeoDA-Inf	A gradient update with horizontal and vertical spectral peaks (with a high central spectral power).
P3	Square-Inf	A per-query change with horizontal spectral peaks.
P4	RayS-Inf	A per-query change with vertical spectral peaks (with a high central spectral power).
P5	RayS-Inf	A per-query change with vertical spectral peaks.
LS	-	A generic line search step, where two per-query changes have the same unsigned direction.
IMG	-	An interpolation step between the clean and perturbed images.

Table 1: Procedures discovered from analyzing the traces of 11 attack variants.

## Discover Procedures

When we do not have access to the attack’s source code, we have to discover the procedures from the observed attack trace. Our guiding principle is that procedures produce coherent query sub-sequences in the spectrum space, as illustrated in Figure 5a. Therefore, we cluster the per-query changes, where each cluster represents a standalone procedure. In particular, we adopt a segment-and-merge strategy to obtain the clusters without deciding the number of clusters. We present the algorithm sketch below and defer its details to Appendix A.4 for brevity.

First, we *segment* the query trace into different sub-sequences by identifying change points. Change points, representing abrupt variations in a time series, signal transitions between different states [64]. We identify these change points in our context by detecting the per-query changes significantly dissimilar from the previous step. Figure 5a shows change points in an attack trace. At step  $i$ , the per-query change is given as  $\delta_i$ . The change points are steps where the mean squared error (MSE) distance of the per-query changes between two successive steps exceeds a predefined threshold, denoted as  $\tau_{\text{segment}}$ ; i.e., if  $\text{MSE}(\delta_i - \delta_{i-1}) > \tau_{\text{segment}}$ .

Second, we *merge* sub-sequences that are statistically similar. This can be done by merging sub-sequences whose means are close:  $\text{MSE}(\bar{\delta}_i - \bar{\delta}_j) < \tau_{\text{merge}}$ , where  $\bar{\delta}_i$  and  $\bar{\delta}_j$  are the means points of two sub-sequences (from the segment step), and  $\tau_{\text{merge}}$  is a pre-defined system threshold.

This process separates the attack trace into multiple clusters of per-query changes. Each cluster  $\mathbb{C} = \{\delta_{i_1}, \delta_{i_2}, \dots\}$  contains queries (or their corresponding per-query changes) that are determined to result from the same prospective procedure. For example, we illustrate in Figure 5a that the two sub-sequences of line search are merged into one cluster.

## Model Procedures

Having identified clusters that describe potential procedures, the next steps are to determine their procedure type and estimate the emission probabilities.

In noise procedures, attacks add i.i.d noise to each query. If a cluster represents a noise procedure, the included queries are clipped images plus noise. When taking the per-query changes, most image content will be removed, and the noise difference will remain. In the spectrum space, the per-query changes will manifest similarly to white noise with a near-constant power spectral density. We binarize the power spectral

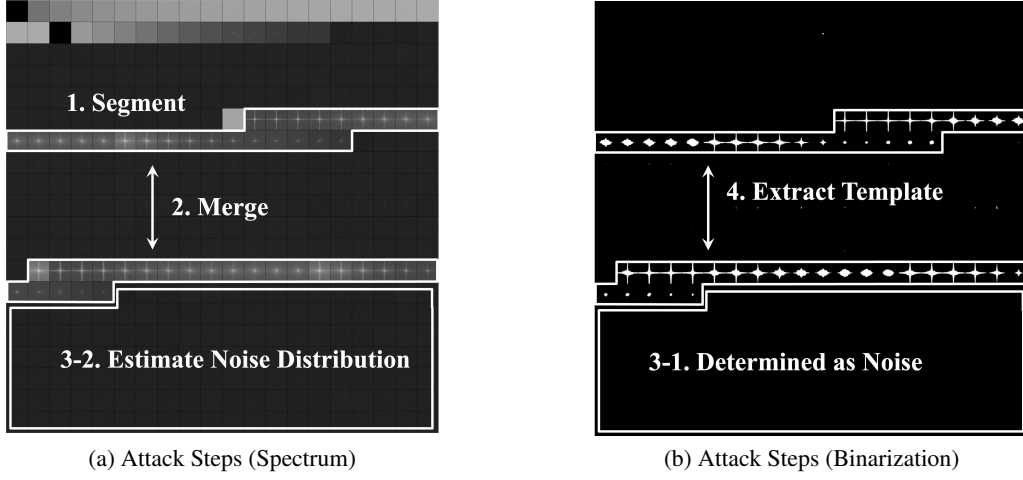


Figure 5: The first 400 steps (i.e., per-query changes) of the GeoDA attack, shown in the spectrum space before and after applying image binarization.

density of the per-query changes in each cluster. As illustrated in Figure 5b, the spectrum has no peaks when its binarized counterpart's  $\ell_0$  norm is close to zero. Recall that the noise procedure's emission probability is defined by the pixel-level noise distribution (see Section 4.3.1). We apply kernel density estimation (KDE) on  $\mathbb{C}$  to estimate the pixel's distribution  $\mathcal{P}'$  and instantiate Equation (2). This process corresponds to Step-3 in Figure 5b.

We determine other clusters, where the average spectral density of the per-query changes have peaks, as corresponding to pattern procedures. We then extract the pattern templates for such procedures as the average binarized power spectral density of the per-query changes in each cluster, as illustrated in Step-4 of Figure 5b. This template instantiates  $\tau$  in Equation (3).

### Enroll Procedures

So far, we have obtained a set of candidate procedures  $\mathbb{P}' = \{\mathbb{P}_i\}_{i=1}^k$ , where each procedure  $\mathbb{P}_i$  has its PMF  $P_i(\mathbf{x})$  estimated from its output per-query changes  $\mathbb{C}_i$ . At this point, we can choose to enroll all discovered procedures into the procedure database. However, this will make the HMM more complex and might affect its generalization. Therefore, we employ a greedy pruning algorithm to choose which procedures from  $\mathbb{P}'$  to enroll.

In particular, each cluster is associated with a potential procedure. We check if the current database  $\mathbb{P}$  contains a procedure that already represents the candidate cluster. We enroll the candidate  $\mathbb{P}_i$  if it improves the estimation of the emission probability as follows:

$$\text{gain} := \frac{1 - \Pr[\mathbb{C}_i | \mathbb{P}_i]}{1 - \max_{\mathbb{P} \in \mathbb{P}} \Pr[\mathbb{C}_i | \mathbb{P}]}, \quad (11)$$

where  $\Pr[\mathbb{C}_i | \mathbb{P}_j] = \prod_{\delta \in \mathbb{C}_i} P_j(\delta)$  is the probability of observing cluster  $\mathbb{C}_i$  under procedure  $\mathbb{P}_j$ , and  $\text{gain}$  measures how much would the candidate  $\mathbb{P}$  improve over existing procedures in the database. We only include the candidate procedure  $\mathbb{P}$  in the database if  $\text{gain} > 10\%$ .

## Enroll Attacks

Having constructed the procedure database, we enroll the attack by estimating the attack’s transition probability  $A$  from the given trace. This is equivalent to generating a fingerprint of the attack as we described in Section 5.3. Table 1 shows the procedures that we have discovered from analyzing the traces of a set of known attacks in literature. These discovered procedures correspond to attack stages, as illustrated in the table. Figure 4 shows the transition matrices of a set of attacks. One could observe how different variants of the same attack appear more visually similar to each other than other attacks.

## 7 Evaluations

We evaluate *SEA* using a variety of attacks, datasets, and models. We outline the experiments and their key findings:

1. **Attribution and Sharing.** *SEA* can fingerprint an attack on its first occurrence and recognize subsequent occurrences of the same attack accurately on multiple datasets and models.
2. **Explanation.** *SEA* can explain the attack’s behavior at a per-query granularity, which leads us to discover very specific implementation bugs in attack libraries.
3. **Robustness.** *SEA* is robust to several adaptive strategies that aim to evade forensics analysis. Such strategies can be recognized as new attacks with high accuracy after a few occurrences.

### 7.1 Setup

We apply *SEA* to analyze query-based black-box attacks against image classification tasks.

#### Datasets and Models

We consider three image classification datasets: ImageNet [55], CelebA [41], and CIFAR10 [37]. We summarize the details of these datasets and the models we used (listed in Table 2) in Appendix B.1.

#### Attack Configuration

We consider 11 black-box attacks and variants: *HSJ-2*, *HSJ-Inf*, *GeoDA-2*, *GeoDA-Inf*, *SignOPT-2*, *Square-2*, *Square-Inf*, *Boundary-2*, *ECO-2*, *RayS-Inf*, and *NES-2*, where *2* and *Inf* indicate each attack’s optimized norm distance. We did not include these two norms for all attacks because they do not support or distinguish that norm. For *CIFAR10*, we randomly select 500 images from the test split as the clean image of all attacks. For *ImageNet* and *CelebA*, we randomly select 200 images due to their high computation costs. We run each attack until it succeeds or reaches 1000 queries.

We evaluate attacks implemented by the open-source ART [46] and BBB [51] libraries. All attacks are evaluated with their default parameters stated in the original paper or recommended by the library. We set the perturbation budget  $\epsilon$  to  $4/255$  for  $\ell_\infty$  and 10 for  $\ell_2$ . Further details of these attacks can be found in Appendix B.2.



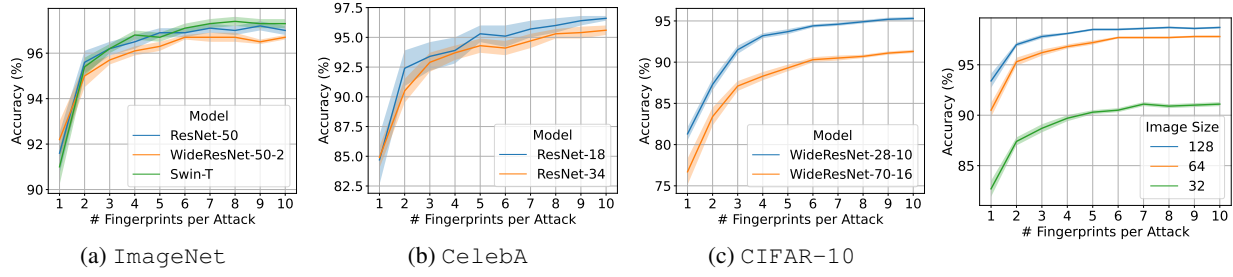


Figure 6: Top-1 accuracy of fingerprint matching as the number of available fingerprints increases for each attack.

## System Configuration

We initialize the databases of SEA with only one attack trace from each of the 11 black-box attacks. This setting resembles a challenging scenario where each attack is reported only once, and SEA needs to deal with their second occurrence. We also evaluate the long-term performance with more traces available. We quantify performance by the accuracy of SEA attributing traces to their ground-truth source attacks. We measure extraction’s precision and recall by mixing the trace with 1000 randomly sampled images from ImageNet.

## 7.2 Evaluation of Attribution and Sharing

We first evaluate the attribution performance of SEA and whether the fingerprints it generates are stable.

### 7.2.1 Attribution via Single Fingerprint

We start with a challenging scenario where SEA fingerprints the attack from only a single trace. We characterize SEA’s attribution of the attack’s second occurrence. Toward that end, we randomly sample one trace from each attack to initialize the attack database of SEA, and then directly use SEA to attribute the remaining traces from all attacks. We repeat the process 100 times and report the accuracy in Table 2. SEA can generally attribute attacks with 90+% Top-1 accuracy and 95+% Top-3 accuracy. The Top-1 accuracy drops slightly on the low-resolution dataset CIFAR10.

### 7.2.2 Attribution via Multiple Fingerprints

As SEA collects more fingerprints for each attack, it also obtains a better estimation of each attack’s probability distribution. This allows us to refine the attack attribution problem using the cosine similarity between a new given fingerprint and the average of available fingerprints. Thus, we evaluate the attribution performance by fingerprint matching as described in Equation (10). Since each fingerprint is generated independently, SEA can scale the probability estimation of each attack without updating its procedure or attack databases.

Figure 6 shows the attribution accuracy by matching a new trace’s fingerprint with the averaged fingerprint of each attack. As SEA collects more fingerprints for each attack, the attribution accuracy quickly converges to 95+% for ImageNet and 90+% for CIFAR10.

Task	Model	Top-1 Acc (%)	Top-3 Acc (%)
ImageNet	ResNet-50	$92.5 \pm 0.5$	$97.2 \pm 0.6$
	WRN-50-2	$92.8 \pm 0.8$	$97.6 \pm 0.5$
	Swin-T	$91.0 \pm 0.3$	$97.1 \pm 0.2$
CelebA	ResNet-18	$91.6 \pm 1.8$	$93.3 \pm 1.3$
	ResNet-34	$92.3 \pm 1.3$	$95.2 \pm 0.9$
CIFAR10	WRN-28-10	$82.6 \pm 0.9$	$95.7 \pm 0.4$
	WRN-70-16	$80.1 \pm 0.5$	$92.7 \pm 0.3$

Table 2: Attributing attacks on their second occurrence.

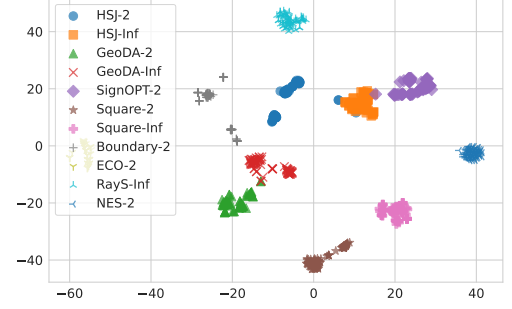


Figure 8: The t-SNE visualization of fingerprints for each attack.

### 7.2.3 Fingerprint Stability

Responsive sharing of an attack’s behavior requires generating a distinguishable fingerprint of the trace on its first occurrence. In this experiment, we evaluate the fingerprint’s stability and distinguishability. For each attack, we generate fingerprints for 100 randomly sampled traces on ImageNet and ResNet-50. This process resembles a scenario where the same attack is (independently) observed multiple times, and SEA should make sure each individual incident would lead to a consistent fingerprint. Figure 11 in Appendix B.4 shows that the fingerprints of each attack are distinguishable with a small confidence interval. Figure 8 shows the t-SNE visualization of the obtained fingerprints for all attacks we studied. We observe distinct clusters of fingerprints, each corresponding to a different attack. Interestingly, variants of the same attack appear closer to each other than other attacks.

## 7.3 Case Studies of Explanation

SEA provides explainability by decoding the behavior of a given trace’s underlying attack. After attributing the attack trace to a specific attack, SEA further attributes each query to a procedure as we explained in Section 5.2.2. Decoding the underlying procedure sequence allows the forensic analyst to form an intuitive understanding of the attack’s behavior and reconfirm the attribution result.

In this experiment, we leverage the explainability of SEA to compare the same attack algorithm’s behavior between two open-source attack libraries, ART and BBB. This would identify potential artifacts between different implementations of the same attack. For each attack, we randomly sample a clean image from ImageNet and generate two attack traces using ART and BBB, respectively. We then apply SEA to decode the trace’s underlying procedure sequence.

Analyzing the decoded procedures, we identify two attacks exhibiting different behavior between these two libraries, even if the attack was given the same set of hyper-parameters. Further inspection of this different behavior leads us to identify and report three bugs in the ART library.

### 7.3.1 Explaining SignOPT Attack

We randomly sample a clean image  $x$  and generate two attack traces using the SignOPT-2 attack from ART and BBB, respectively. SEA successfully attributes both traces to the SignOPT-2 attack and provides the decoded procedure sequences in Figure 9.

For the first 500 queries, all three traces exhibit similar behavior with a frequent transition between N4

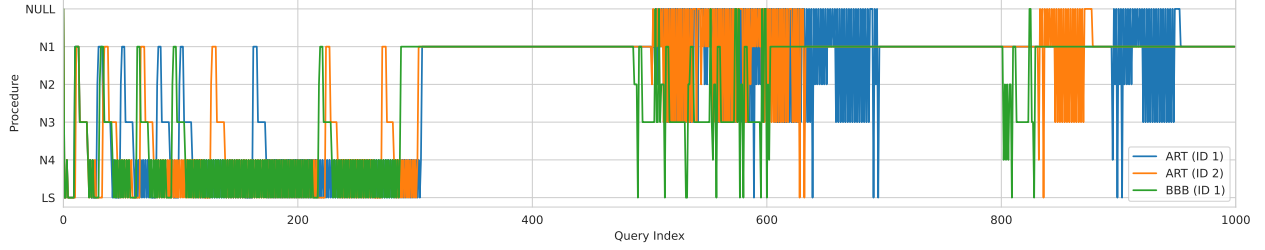


Figure 9: Decoded behavior of the `SignOPT-2` attack implemented by the ART and BBB libraries. The traces of two different clean inputs from the ART library exhibit consistent behavior. But traces of the same clean input (ID 1) from ART and BBB exhibit different patterns in the middle (index 500–700).

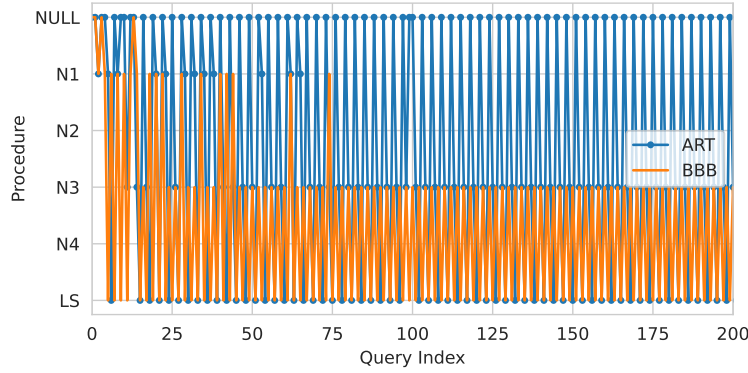


Figure 10: Decoded behavior of the `Square-2` attack implemented by the ART and BBB libraries. The traces of the same clean input from ART and BBB exhibit different patterns everywhere.

and `LS` that ends with a constant `N1`. This observation is consistent with the attack’s algorithm, which keeps sampling noise and uses binary search to initialize the adversarial direction.

However, starting from the 500-th query, the ART variant shows a frequent transition to `NULL`, which is not observed in the BBB variant. This observation implies that the ART variant keeps producing duplicated queries. After examining its source code, we successfully locate the following bug:

```
if (not adv(x) and flag) or (adv(x) and not flag):
    ...
else:
    ...
```

where the same query request `adv(x)` is executed twice when `flag = False`. Once we fixed this bug, the resulting attack trace exhibited the same behavior as BBB.

### 7.3.2 Explaining Square Attack

Similarly, we repeat the above process using the `Square-2` attack implemented by ART and BBB, respectively. SEA successfully attributes both traces to the `Square-2` attack and provides the decoded behavior in Figure 10. We omit the reference trace from ART because it overlaps with the other one from ART.

Again, both traces exhibit similar behavior except ART’s additional frequent transition to `NULL`. After examining the source code, we successfully locate two performance bugs where the previous query results

Attack	Precision (%)			Recall (%)		
	0.4	0.5	0.6	0.4	0.5	0.6
HSJ-2	98.9	100.0	100.0	99.9	99.8	94.3
HSJ-Inf	98.9	100.0	100.0	99.8	99.7	82.8
GeoDA-2	98.9	100.0	100.0	100.0	94.0	88.6
GeoDA-Inf	98.8	100.0	100.0	99.5	99.4	99.2
Square-2	98.7	100.0	100.0	90.0	90.0	90.0
Square-Inf	95.3	99.9	100.0	98.5	98.5	98.5
SignOPT-2	98.1	99.9	100.0	100.0	100.0	100.0
Bound-2	98.9	100.0	100.0	99.9	99.9	99.9
ECO-2	98.9	100.0	100.0	100.0	100.0	100.0
NES-2	98.8	100.0	100.0	82.5	77.4	73.3
RayS-Inf	98.9	100.0	100.0	100.0	100.0	100.0

Table 3: Performance of trace extraction with varying thresholds ( $r \in \{0.4, 0.5, 0.6\}$ ).

could have been reused under certain conditions. The detailed analysis can be found in Appendix B.3. The attack trace from ART resembles BBB once we fixed these two performance bugs.

### Takeaway

The above case studies confirm the explainability of SEA beyond simply attributing the attack’s identity. In practice, the forensic analyst may not have access to the attack’s source code, but SEA can still provide more insights into the attack’s behavior and assist the potential need to replicate the attack. The explanation also benefits identifying artifacts correlated with the attack’s toolchain. For example, one could infer the attacker’s toolkit if such artifacts were reported elsewhere. Deep learning methods cannot identify such artifacts, as the final adversarial examples remain identical. We reported these bugs to ART for performance improvements, and one of them has been fixed.

## 7.4 Ablation Studies

We now provide two ablation studies for attribution with incomplete traces and down-scaled traces.

### 7.4.1 Attribution with Incomplete Traces

So far, we have been extracting the trace using a fixed threshold  $r = 0.5$  in Section 5.1. For completeness, we evaluate the extraction and attribution performance with other values. Table 3 shows the extraction’s precision and recall on each attack. For  $r = 0.4$  the precision is imperfect, yet setting  $r = 0.6$  will decrease the recall. We thus choose  $r = 0.5$  to achieve a high recall while keeping 100% precision. We then evaluate the overall performance with different thresholds in Table 4, aggregating the performance over all attacks. Increasing the threshold further will extract an incomplete trace, leading to a slightly worse attribution performance.

### 7.4.2 Reducing the Storage Cost

Storing history queries introduce an inevitable storage cost. SEA provides an option to store the down-scaled queries and conduct attribution at a minor cost of performance. We evaluate attribution on ImageNet and ResNet-50, with the original queries down-scaled to size  $128 \times 128$ ,  $64 \times 64$ , and  $32 \times 32$ . As shown

$r$	Extraction (%)		Attribution (%)	
	Precision	Recall	Top-1 Acc	Top-3 Acc
0.5	100.0 $\pm$ 0.0	96.2 $\pm$ 0.2	92.5 $\pm$ 0.5	97.2 $\pm$ 0.6
0.6	100.0 $\pm$ 0.0	93.3 $\pm$ 0.1	91.2 $\pm$ 1.2	96.0 $\pm$ 0.8
0.7	100.0 $\pm$ 0.0	92.5 $\pm$ 0.6	90.2 $\pm$ 1.2	95.3 $\pm$ 0.8
0.8	100.0 $\pm$ 0.0	90.1 $\pm$ 0.9	88.3 $\pm$ 1.1	94.0 $\pm$ 0.7
0.9	100.0 $\pm$ 0.0	88.7 $\pm$ 1.2	83.9 $\pm$ 1.0	91.1 $\pm$ 0.7

Table 4: Performance of attribution on incomplete traces.

in Figure 7, reducing the image size has a clear impact on the performance. This is because the lossy compression inevitably makes the trace harder to distinguish. But this can be relieved if more fingerprints are available, where even  $32 \times 32$  can preserve 90% Top-1 accuracy.

## 7.5 Adaptive Attacks

We also consider attacks that are aware of our system and attempt to obfuscate or evade our analysis with adaptive strategies. We explore potential such strategies and evaluate SEA’s performance when they are deployed.

Since SEA performs forensic analysis post-attack, it can adapt to new adaptive attacks by incorporating them into its database. We emulate this process by evaluating the attack’s first and second occurrences. For each attack, we evaluate how SEA performs before and after it has observed and reacted to the adaptive strategy.

### 7.5.1 Sending Dummy Queries

A simple strategy for obfuscation is hiding the attack’s trace within a large number of dummy queries. The attack will ignore the prediction of these dummy queries so its performance is unaffected. The attack also ensures that such dummy queries are correlated with the final adversarial example so SEA will include them in the attack trace.

One example of dummy queries is randomly duplicating the queries. This scenario is covered by our evaluation of explainability in Section 7.3, where the ART library happens to provide such variants because of implementation artifacts. For the SignOPT and Square attacks, SEA can correctly attribute and explain such attacks even when they have included duplicated queries.

We then consider sending dummy queries perturbed by Gaussian noise. For each batch of queries  $\{\mathbf{x}_t\}_{t=i}^j$ , the attack will mix them with a noisy counterpart  $\{\mathbf{x}_t + \boldsymbol{\eta}_t\}_{t=i}^j$ , where  $\boldsymbol{\eta}_t \stackrel{\text{iid}}{\sim} \mathcal{N}(\mathbf{0}_d, \sigma^2 \mathbf{I}_d)$  is the added Gaussian noise. We take the HSJ-2 attack as an example because its original version leverages Gaussian noise to estimate gradients, thus more likely to create an obfuscation. We test different noise levels by adjusting  $\sigma$  and report the results in Table 5.

On the adaptive attack’s first occurrence, SEA can only attribute around 59% of such traces to the HSJ-2 attack, although a 95% Top-3 accuracy bounds the confusion. This is expected because the attack has effectively changed its behavior. However, once SEA has added the newly observed attack’s fingerprint to its database, it recognizes this variant on the second occurrence with 100% accuracy.

Noise ( $\sigma$ )	First Occurrence (%)		Second Occurrence (%)	
	Top-1	Top-3	Top-1	Top-3
0.00	93.3 $\pm$ 0.9	98.9 $\pm$ 0.1	100.0 $\pm$ 0.0	100.0 $\pm$ 0.0
0.05	58.4 $\pm$ 3.3	95.8 $\pm$ 0.7	100.0 $\pm$ 0.0	100.0 $\pm$ 0.0
0.10	56.1 $\pm$ 3.1	93.7 $\pm$ 0.7	100.0 $\pm$ 0.0	100.0 $\pm$ 0.0
0.15	59.1 $\pm$ 3.9	94.3 $\pm$ 0.8	100.0 $\pm$ 0.0	100.0 $\pm$ 0.0
0.20	58.5 $\pm$ 4.0	94.4 $\pm$ 0.7	100.0 $\pm$ 0.0	100.0 $\pm$ 0.0

Table 5: Attribution of HSJ with dummy noisy queries.

Noise ( $\sigma$ )	First Occurrence (%)		Second Occurrence (%)	
	Top-1	Top-3	Top-1	Top-3
0.0002	97.1 $\pm$ 1.4	100.0 $\pm$ 0.0	100.0 $\pm$ 0.0	100.0 $\pm$ 0.0
0.002	95.7 $\pm$ 2.2	100.0 $\pm$ 0.0	100.0 $\pm$ 0.0	100.0 $\pm$ 0.0
0.02	83.2 $\pm$ 6.2	100.0 $\pm$ 0.0	100.0 $\pm$ 0.0	100.0 $\pm$ 0.0
0.2	80.1 $\pm$ 3.1	100.0 $\pm$ 0.0	100.0 $\pm$ 0.0	100.0 $\pm$ 0.0
2.0	56.7 $\pm$ 8.6	99.8 $\pm$ 0.2	100.0 $\pm$ 0.0	100.0 $\pm$ 0.0

Table 6: Attribution of GeoDA with increased noise.

### 7.5.2 Increasing the Noise Magnitude

Because SEA relies on the noise distribution of the per-query changes, an adaptive attack might attempt to obfuscate its identity by adjusting its noise magnitude. We consider the case where a GeoDA-2 attack attempts to obfuscate its identity by increasing its noise magnitude used for gradient estimation. We increase the attack’s noise magnitude  $\sigma$  up to a factor of  $10^4$  and report the results in Table 6.

On the attack’s first occurrence, SEA indeed attributes the adaptive GeoDA-2 attack with a lower Top-1 accuracy. This means the adaptive strategy can successfully obfuscate the attack’s identity, although the overall obfuscation is limited due to a high Top-3 accuracy.

Once SEA has added the newly observed attack’s fingerprint to its database, it recognizes this variant on the second occurrence with 100% accuracy. This result suggests that obfuscating an attack’s identity (or even forging another one) is challenging under SEA, because the attack has to adjust not only the distribution of each single query but also the overall behavior pattern.

### 7.5.3 Increasing the Learning Rates

Attacks might also want to increase their learning rates as an attempt to increase the changes between queries, thereby obfuscating their behavior under SEA. We explore this adaptive strategy for NES-2, HSJ-2, and HSJ-Inf attacks because they have explicit control over the learning rates. For the NES-2 attack, we gradually increase its learning rate from 1 to 1000 where the attack reaches 0% success rate. SEA can extract the entire query sequence with 100% precision and recall while attributing all such traces to the NES-2 attack.

Since HSJ-2 and HSJ-Inf attacks use binary search to determine the step size, we remove their binary search process and use a fixed learning rate up to 1000. The attribution remains 98% accuracy. We confirm by visualization that the two attacks also rely on another binary search process that dominates their behavior. Further removing this process makes the attack unreasonable and effectively changes its behavior, but SEA can recognize this variant with 100% accuracy after adding its fingerprint to the database.

Attack	Extraction (%)		Attribution (%)	
	Precision	Recall	$k = 1$	$k = 5$
HSJ-2	$99.4 \pm 0.3$	$69.2 \pm 4.6$	$63.4 \pm 2.5$	$90.4 \pm 0.9$
HSJ-Inf	$99.1 \pm 0.4$	$67.3 \pm 4.7$	$70.5 \pm 2.2$	$94.0 \pm 0.7$
GeoDA-2	$99.2 \pm 0.3$	$61.1 \pm 5.3$	$67.2 \pm 2.8$	$92.7 \pm 0.7$
GeoDA-Inf	$99.3 \pm 0.3$	$67.3 \pm 4.7$	$78.3 \pm 2.2$	$96.9 \pm 0.5$
SignOPT-2	$99.2 \pm 0.4$	$68.9 \pm 4.5$	$61.5 \pm 2.4$	$92.1 \pm 0.9$
Square-2	$96.5 \pm 1.8$	$73.9 \pm 4.7$	$70.6 \pm 2.4$	$92.7 \pm 0.9$
Square-Inf	$97.8 \pm 1.3$	$75.4 \pm 4.8$	$71.5 \pm 2.4$	$94.2 \pm 0.8$
Boundary-2	$99.2 \pm 0.4$	$64.3 \pm 4.4$	$82.6 \pm 2.3$	$93.6 \pm 0.4$
ECO-2	$99.1 \pm 0.4$	$76.6 \pm 4.6$	$71.6 \pm 2.2$	$93.6 \pm 0.9$
RayS-Inf	$98.9 \pm 0.5$	$45.7 \pm 6.1$	$54.8 \pm 2.5$	$92.6 \pm 0.9$
NES-2	$99.3 \pm 0.3$	$73.6 \pm 4.7$	$70.2 \pm 2.4$	$94.4 \pm 0.7$

Table 7: Performance of extracting and recognizing the image transformation adaptive attack with  $k$  traces.

### 7.5.4 Applying Image Transformation

Since our system relies on the characterization of changes between queries, the attack can attempt to make such characterizations harder by applying transformations to their queries, e.g., shifting and rotation. Although our threat model focuses on norm-bounded attacks where applying such transformations is currently intractable, we show that SEA can still recognize this obfuscation technique without any adaptation.

We explore randomized rotation with  $\theta_t \sim [-10^\circ, 10^\circ]$  degrees for each query  $\mathbf{x}_t$ . Given such transformed queries, a direct extraction as described in Section 5.1 leads to around 99% precision and 65–75% recall for all attacks, with detailed results in Table 7. By adding up to five fingerprints of such traces to the database, SEA can reliably recognize this technique with 90+% accuracy. At this point, any attack applying the rotation technique has become a new group of attacks and is recognized by SEA thereafter.

### Takeaway

We observe that adaptive strategies can evade fingerprinting in their first occurrence at an increased cost. Sending dummy queries, increasing the noise magnitude, and increasing the learning rates will result in more issued queries. Applying image transformations will increase the  $\ell_p$  norm of the perturbation. It is possible to conceive other adaptive strategies that have better query/perturbation budgets. Still, employing adaptive strategies change the nature of the attack so that SEA treats them as different attacks and will eventually fingerprint them. The attacker, even when adaptive, remains at a disadvantage because they cannot change the observed trace post-attack.

## 8 Discussions

### Machine Learning-aware Logging

Logs are a foundational building block of modern computing – they aid with routine system checks and recovery. At the same time, the logging of ML systems is under-explored. What should be kept in place to enable effective recovery of crashed systems or systems that violated the underlying safety/security policy? Our paper designs a first logging-forensic foundation for long-term ML deployment. We find that, to adapt and track our adversaries, book-keeping of individual user-query behaviors is required. While much of the current policy discussion revolves around auditing of systems at the design phase [6], the current draft of the

EU Artificial Intelligence Act [2] has no mentions of logging or continuous system monitoring. We argue that explicit policies should be developed to promise long-term monitoring, threat intelligence sharing, and management of ML deployments.

### **Manual Overhead for Adding New Attacks**

Section 6 described two approaches to enroll new attacks into SEA. Both approaches require manual intervention to analyze source code or model the procedures. Our semi-automated approach to discovering the procedures and, subsequently, attacks involves some amount of manual intervention. One author enrolled the attacks in our experiments one trace at a time. Adding a single trace takes a few minutes. The additional manual overhead arises from visually confirming the clustering results, tuning the hyper-parameter if necessary, and including the automatically extracted PMF and template in the code. However, a higher level of manual analysis is needed if the user wants to discover more abstract procedures, such as line search and interpolation. These were the only special procedures we found in existing attacks.

## **9 Conclusion**

SEA is the first ML security system designed to analyze black-box attacks against ML systems for forensic purposes and enable human-explainable intelligence sharing. We demonstrate on a variety of attacks and settings that SEA can characterize an attack on its first occurrence and accurately recognize subsequent occurrences of the same attack. More importantly, the attribution it provides is understandable by humans. Future work may explore the application of SEA to other domains and refine its trace preservation and extraction process. Other research thrusts include enhancing automation to reduce human involvement and investigating robustness against more adaptive attacks.



## References

- [1] CVE List from MITRE. <https://cve.mitre.org/>, 2023.
- [2] EU Artificial Intelligence Act. [https://www.europarl.europa.eu/thinktank/en/document/EPRS\\_BRI\(2021\)698792](https://www.europarl.europa.eu/thinktank/en/document/EPRS_BRI(2021)698792), 2023.
- [3] US CERT. <https://www.cisa.gov/>, 2023.
- [4] Milad Taleby Ahvanooey, Qianmu Li, Xuefang Zhu, Mamoun Alazab, and Jing Zhang. Anitw: A novel intelligent text watermarking technique for forensic identification of spurious information on social media. *Computers & Security*, 90:101702, 2020.
- [5] Manjushree B. Aithal and Xiaohua Li. Boundary defense against black-box adversarial attacks. *CoRR*, abs/2201.13444, 2022.
- [6] Markus Anderljung, Joslyn Barnhart, Anton Korinek, Jade Leung, Cullen O’Keefe, Jess Whittlestone, Shahar Avin, Miles Brundage, Justin Bullock, Duncan Cass-Beggs, Ben Chang, Tantum Collins, Tim Fist, Gillian Hadfield, Alan Hayes, Lewis Ho, Sara Hooker, Eric Horvitz, Noam Kolt, Jonas Schuett, Yonadav Shavit, Divya Siddarth, Robert Trager, and Kevin Wolf. Frontier ai regulation: Managing emerging risks to public safety, 2023.
- [7] Maksym Andriushchenko, Francesco Croce, Nicolas Flammarion, and Matthias Hein. Square attack: A query-efficient black-box adversarial attack via random search. In Andrea Vedaldi, Horst Bischof, Thomas Brox, and Jan-Michael Frahm, editors, *Computer Vision - ECCV 2020 - 16th European Conference, Glasgow, UK, August 23-28, 2020, Proceedings, Part XXIII*, volume 12368 of *Lecture Notes in Computer Science*, pages 484–501. Springer, 2020.
- [8] Anish Athalye, Nicholas Carlini, and David A. Wagner. Obfuscated gradients give a false sense of security: Circumventing defenses to adversarial examples. In Jennifer G. Dy and Andreas Krause, editors, *Proceedings of the 35th International Conference on Machine Learning, ICML 2018, Stockholmsmässan, Stockholm, Sweden, July 10-15, 2018*, volume 80 of *Proceedings of Machine Learning Research*, pages 274–283. PMLR, 2018.
- [9] Battista Biggio, Igino Corona, Davide Maiorca, Blaine Nelson, Nedim Srndic, Pavel Laskov, Giorgio Giacinto, and Fabio Roli. Evasion attacks against machine learning at test time. In Hendrik Blockeel, Kristian Kersting, Siegfried Nijssen, and Filip Zelezný, editors, *Machine Learning and Knowledge Discovery in Databases - European Conference, ECML PKDD 2013, Prague, Czech Republic, September 23-27, 2013, Proceedings, Part III*, volume 8190 of *Lecture Notes in Computer Science*, pages 387–402. Springer, 2013.
- [10] Wieland Brendel, Jonas Rauber, and Matthias Bethge. Decision-based adversarial attacks: Reliable attacks against black-box machine learning models. In *6th International Conference on Learning Representations, ICLR 2018, Vancouver, BC, Canada, April 30 - May 3, 2018, Conference Track Proceedings*. OpenReview.net, 2018.
- [11] Junyoung Byun, Hyojun Go, and Changick Kim. On the effectiveness of small input noise for defending against query-based black-box attacks. In *IEEE/CVF Winter Conference on Applications of Computer Vision, WACV 2022, Waikoloa, HI, USA, January 3-8, 2022*, pages 3819–3828. IEEE, 2022.

- [12] Nicholas Carlini and David A. Wagner. Towards evaluating the robustness of neural networks. In *2017 IEEE Symposium on Security and Privacy, SP 2017, San Jose, CA, USA, May 22-26, 2017*, pages 39–57, 2017.
- [13] Jianbo Chen, Michael I. Jordan, and Martin J. Wainwright. Hopskipjumpattack: A query-efficient decision-based attack. In *2020 IEEE Symposium on Security and Privacy, SP 2020, San Francisco, CA, USA, May 18-21, 2020*, pages 1277–1294. IEEE, 2020.
- [14] Jinghui Chen and Quanquan Gu. Rays: A ray searching method for hard-label adversarial attack. In Rajesh Gupta, Yan Liu, Jiliang Tang, and B. Aditya Prakash, editors, *KDD '20: The 26th ACM SIGKDD Conference on Knowledge Discovery and Data Mining, Virtual Event, CA, USA, August 23-27, 2020*, pages 1739–1747. ACM, 2020.
- [15] Pin-Yu Chen, Huan Zhang, Yash Sharma, Jinfeng Yi, and Cho-Jui Hsieh. Zoo: Zeroth order optimization based black-box attacks to deep neural networks without training substitute models. In *Proceedings of the 10th ACM workshop on artificial intelligence and security*, pages 15–26, 2017.
- [16] Sizhe Chen, Zhehao Huang, Qinghua Tao, Yingwen Wu, Cihang Xie, and Xiaolin Huang. Adversarial attack on attackers: Post-process to mitigate black-box score-based query attacks. *CoRR*, abs/2205.12134, 2022.
- [17] Steven Chen, Nicholas Carlini, and David A. Wagner. Stateful detection of black-box adversarial attacks. *CoRR*, abs/1907.05587, 2019.
- [18] Minhao Cheng, Thong Le, Pin-Yu Chen, Huan Zhang, Jinfeng Yi, and Cho-Jui Hsieh. Query-efficient hard-label black-box attack: An optimization-based approach. In *7th International Conference on Learning Representations, ICLR 2019, New Orleans, LA, USA, May 6-9, 2019*. OpenReview.net, 2019.
- [19] Minhao Cheng, Simranjit Singh, Patrick H. Chen, Pin-Yu Chen, Sijia Liu, and Cho-Jui Hsieh. Sign-opt: A query-efficient hard-label adversarial attack. In *8th International Conference on Learning Representations, ICLR 2020, Addis Ababa, Ethiopia, April 26-30, 2020*. OpenReview.net, 2020.
- [20] Francesco Croce, Maksym Andriushchenko, Vikash Sehwal, Edoardo Debenedetti, Nicolas Flammarion, Mung Chiang, Prateek Mittal, and Matthias Hein. Robustbench: a standardized adversarial robustness benchmark. In *Thirty-fifth Conference on Neural Information Processing Systems Datasets and Benchmarks Track*, 2021.
- [21] Edoardo Debenedetti, Nicholas Carlini, and Florian Tramèr. Evading black-box classifiers without breaking eggs. *arXiv preprint arXiv: 2306.02895*, 2023.
- [22] Feng Ding, Guopu Zhu, Yingcan Li, Xinpeng Zhang, Pradeep K. Atrey, and Siwei Lyu. Anti-forensics for face swapping videos via adversarial training. *IEEE Trans. Multim.*, 24:3429–3441, 2022.
- [23] Yinpeng Dong, Tianyu Pang, Hang Su, and Jun Zhu. Evading defenses to transferable adversarial examples by translation-invariant attacks. In *IEEE Conference on Computer Vision and Pattern Recognition, CVPR 2019, Long Beach, CA, USA, June 16-20, 2019*, pages 4312–4321. Computer Vision Foundation / IEEE, 2019.
- [24] Marissa Dotter, Sherry Xie, Keith Manville, Josh Harguess, Colin Busho, and Mikel Rodriguez. Adversarial attack attribution: Discovering attributable signals in adversarial ML attacks. *CoRR*, abs/2101.02899, 2021.

- [25] Martin Ester, Hans-Peter Kriegel, Jörg Sander, and Xiaowei Xu. A density-based algorithm for discovering clusters in large spatial databases with noise. In *Proceedings of the Second International Conference on Knowledge Discovery and Data Mining*, KDD'96, page 226–231. AAAI Press, 1996.
- [26] Peng Fei, Zhou Li, Zhiying Wang, Xiao Yu, Ding Li, and Kangkook Jee. {SEAL}: Storage-efficient causality analysis on enterprise logs with query-friendly compression. In *30th USENIX Security Symposium (USENIX Security 21)*, pages 2987–3004, 2021.
- [27] G.D. Forney. The viterbi algorithm. *Proceedings of the IEEE*, 61(3):268–278, 1973.
- [28] Qi-An Fu, Yinpeng Dong, Hang Su, Jun Zhu, and Chao Zhang. AutoDA: Automated decision-based iterative adversarial attacks. In *31st USENIX Security Symposium (USENIX Security 22)*, pages 3557–3574, Boston, MA, August 2022. USENIX Association.
- [29] Yue Gao, Ilia Shumailov, and Kassem Fawaz. Rethinking image-scaling attacks: The interplay between vulnerabilities in machine learning systems. In *Proceedings of the 39th International Conference on Machine Learning*, volume 162 of *Proceedings of Machine Learning Research*, pages 7102–7121, Baltimore, MI, July 2022. PMLR.
- [30] Yue Gao, Ilia Shumailov, Kassem Fawaz, and Nicolas Papernot. On the limitations of stochastic pre-processing defenses. In *Advances in Neural Information Processing Systems 36: Annual Conference on Neural Information Processing Systems 2022, NeurIPS 2022*, 2022.
- [31] Chuan Guo, Jacob R. Gardner, Yurong You, Andrew Gordon Wilson, and Kilian Q. Weinberger. Simple black-box adversarial attacks. In Kamalika Chaudhuri and Ruslan Salakhutdinov, editors, *Proceedings of the 36th International Conference on Machine Learning, ICML 2019, 9-15 June 2019, Long Beach, California, USA*, volume 97 of *Proceedings of Machine Learning Research*, pages 2484–2493. PMLR, 2019.
- [32] Chuan Guo, Mayank Rana, Moustapha Cissé, and Laurens van der Maaten. Countering adversarial images using input transformations. In *6th International Conference on Learning Representations, ICLR 2018, Vancouver, BC, Canada, April 30 - May 3, 2018, Conference Track Proceedings*. OpenReview.net, 2018.
- [33] Zhongyi Guo, Keji Han, Yao Ge, Wei Ji, and Yun Li. Scalable attribution of adversarial attacks via multi-task learning. *CoRR*, abs/2302.14059, 2023.
- [34] Andrew Ilyas, Logan Engstrom, Anish Athalye, and Jessy Lin. Black-box adversarial attacks with limited queries and information. In Jennifer G. Dy and Andreas Krause, editors, *Proceedings of the 35th International Conference on Machine Learning, ICML 2018, Stockholmsmässan, Stockholm, Sweden, July 10-15, 2018*, volume 80 of *Proceedings of Machine Learning Research*, pages 2142–2151. PMLR, 2018.
- [35] Mika Juuti, Sebastian Szyller, Samuel Marchal, and N. Asokan. PRADA: protecting against DNN model stealing attacks. In *IEEE European Symposium on Security and Privacy, EuroS&P 2019, Stockholm, Sweden, June 17-19, 2019*, pages 512–527. IEEE, 2019.
- [36] Samuel T King and Peter M Chen. Backtracking intrusions. In *Proceedings of the nineteenth ACM symposium on Operating systems principles*, pages 223–236, 2003.

- [37] Alex Krizhevsky, Geoffrey Hinton, et al. Learning multiple layers of features from tiny images. 2009.
- [38] Huichen Li, Xiaojun Xu, Xiaolu Zhang, Shuang Yang, and Bo Li. QEBA: query-efficient boundary-based blackbox attack. In *2020 IEEE/CVF Conference on Computer Vision and Pattern Recognition, CVPR 2020, Seattle, WA, USA, June 13-19, 2020*, pages 1218–1227. Computer Vision Foundation / IEEE, 2020.
- [39] Huiying Li, Shawn Shan, Emily Wenger, Jiayun Zhang, Haitao Zheng, and Ben Y. Zhao. Black-light: Scalable defense for neural networks against Query-Based Black-Box attacks. In *31st USENIX Security Symposium (USENIX Security 22)*, pages 2117–2134, Boston, MA, August 2022. USENIX Association.
- [40] Jie Li, Rongrong Ji, Hong Liu, Jianzhuang Liu, Bineng Zhong, Cheng Deng, and Qi Tian. Projection & probability-driven black-box attack. In *2020 IEEE/CVF Conference on Computer Vision and Pattern Recognition, CVPR 2020, Seattle, WA, USA, June 13-19, 2020*, pages 359–368. Computer Vision Foundation / IEEE, 2020.
- [41] Ziwei Liu, Ping Luo, Xiaogang Wang, and Xiaoou Tang. Deep learning face attributes in the wild. In *Proceedings of International Conference on Computer Vision (ICCV)*, December 2015.
- [42] Aleksander Madry, Aleksandar Makelov, Ludwig Schmidt, Dimitris Tsipras, and Adrian Vladu. Towards deep learning models resistant to adversarial attacks. In *6th International Conference on Learning Representations, ICLR 2018, Vancouver, BC, Canada, April 30 - May 3, 2018, Conference Track Proceedings*, 2018.
- [43] Mazda Moayeri and Soheil Feizi. Sample efficient detection and classification of adversarial attacks via self-supervised embeddings. In *2021 IEEE/CVF International Conference on Computer Vision, ICCV 2021, Montreal, QC, Canada, October 10-17, 2021*, pages 7657–7666. IEEE, 2021.
- [44] Seungyong Moon, Gaon An, and Hyun Oh Song. Parsimonious black-box adversarial attacks via efficient combinatorial optimization. In Kamalika Chaudhuri and Ruslan Salakhutdinov, editors, *Proceedings of the 36th International Conference on Machine Learning, ICML 2019, 9-15 June 2019, Long Beach, California, USA*, volume 97 of *Proceedings of Machine Learning Research*, pages 4636–4645. PMLR, 2019.
- [45] David Aaron Nicholson and Vincent Emanuele. Reverse engineering adversarial attacks with fingerprints from adversarial examples. *CoRR*, abs/2301.13869, 2023.
- [46] Maria-Irina Nicolae, Mathieu Sinn, Minh Ngoc Tran, Beat Buesser, Ambrish Rawat, Martin Wistuba, Valentina Zantedeschi, Nathalie Baracaldo, Bryant Chen, Heiko Ludwig, Ian Molloy, and Ben Edwards. Adversarial robustness toolbox v1.2.0. *CoRR*, 1807.01069, 2018.
- [47] Weili Nie, Brandon Guo, Yujia Huang, Chaowei Xiao, Arash Vahdat, and Animashree Anandkumar. Diffusion models for adversarial purification. In Kamalika Chaudhuri, Stefanie Jegelka, Le Song, Csaba Szepesvári, Gang Niu, and Sivan Sabato, editors, *International Conference on Machine Learning, ICML 2022, 17-23 July 2022, Baltimore, Maryland, USA*, volume 162 of *Proceedings of Machine Learning Research*, pages 16805–16827. PMLR, 2022.

- [48] Ren Pang, Xinyang Zhang, Shouling Ji, Xiapu Luo, and Ting Wang. Advmind: Inferring adversary intent of black-box attacks. In Rajesh Gupta, Yan Liu, Jiliang Tang, and B. Aditya Prakash, editors, *KDD '20: The 26th ACM SIGKDD Conference on Knowledge Discovery and Data Mining, Virtual Event, CA, USA, August 23-27, 2020*, pages 1899–1907. ACM, 2020.
- [49] Nicolas Papernot, Patrick D. McDaniel, Ian J. Goodfellow, Somesh Jha, Z. Berkay Celik, and Ananthram Swami. Practical black-box attacks against machine learning. In Ramesh Karri, Ozgur Sinanoglu, Ahmad-Reza Sadeghi, and Xun Yi, editors, *Proceedings of the 2017 ACM on Asia Conference on Computer and Communications Security, AsiaCCS 2017, Abu Dhabi, United Arab Emirates, April 2-6, 2017*, pages 506–519. ACM, 2017.
- [50] Zeyu Qin, Yanbo Fan, Hongyuan Zha, and Baoyuan Wu. Random noise defense against query-based black-box attacks. In Marc’Aurelio Ranzato, Alina Beygelzimer, Yann N. Dauphin, Percy Liang, and Jennifer Wortman Vaughan, editors, *Advances in Neural Information Processing Systems 34: Annual Conference on Neural Information Processing Systems 2021, NeurIPS 2021, December 6-14, 2021, virtual*, pages 7650–7663, 2021.
- [51] Zeyu Qin, Xuanchen Yan, and Baoyuan Wu. Blackboxbench (python library), 2022.
- [52] Lawrence R. Rabiner. A tutorial on hidden markov models and selected applications in speech recognition. *Proc. IEEE*, 77(2):257–286, 1989.
- [53] Edward Raff, Jared Sylvester, Steven Forsyth, and Mark McLean. Barrage of random transforms for adversarially robust defense. In *IEEE Conference on Computer Vision and Pattern Recognition, CVPR 2019, Long Beach, CA, USA, June 16-20, 2019*, pages 6528–6537. Computer Vision Foundation / IEEE, 2019.
- [54] Ali Rahmati, Seyed-Mohsen Moosavi-Dezfooli, Pascal Frossard, and Huaiyu Dai. Geoda: A geometric framework for black-box adversarial attacks. In *2020 IEEE/CVF Conference on Computer Vision and Pattern Recognition, CVPR 2020, Seattle, WA, USA, June 13-19, 2020*, pages 8443–8452. Computer Vision Foundation / IEEE, 2020.
- [55] Olga Russakovsky, Jia Deng, Hao Su, Jonathan Krause, Sanjeev Satheesh, Sean Ma, Zhiheng Huang, Andrej Karpathy, Aditya Khosla, Michael S. Bernstein, Alexander C. Berg, and Fei-Fei Li. Imagenet large scale visual recognition challenge. *Int. J. Comput. Vis.*, 115(3):211–252, 2015.
- [56] Daniel Schlette, Marco Caselli, and Günther Pernul. A comparative study on cyber threat intelligence: The security incident response perspective. *IEEE Communications Surveys & Tutorials*, 23(4):2525–2556, 2021.
- [57] Shawn Shan, Arjun Nitin Bhagoji, Haitao Zheng, and Ben Y. Zhao. Poison forensics: Traceback of data poisoning attacks in neural networks. In Kevin R. B. Butler and Kurt Thomas, editors, *31st USENIX Security Symposium, USENIX Security 2022, Boston, MA, USA, August 10-12, 2022*, pages 3575–3592. USENIX Association, 2022.
- [58] Chawin Sitawarin, Zachary J. Golan-Strieb, and David A. Wagner. Demystifying the adversarial robustness of random transformation defenses. In Kamalika Chaudhuri, Stefanie Jegelka, Le Song, Csaba Szepesvári, Gang Niu, and Sivan Sabato, editors, *International Conference on Machine Learning, ICML 2022, 17-23 July 2022, Baltimore, Maryland, USA*, volume 162 of *Proceedings of Machine Learning Research*, pages 20232–20252. PMLR, 2022.

- [59] Matthew C. Stamm, W. Sabrina Lin, and K. J. Ray Liu. Temporal forensics and anti-forensics for motion compensated video. *IEEE Trans. Inf. Forensics Secur.*, 7(4):1315–1329, 2012.
- [60] Matthew C. Stamm and K. J. Ray Liu. Anti-forensics of digital image compression. *IEEE Trans. Inf. Forensics Secur.*, 6(3-2):1050–1065, 2011.
- [61] Christian Szegedy, Wojciech Zaremba, Ilya Sutskever, Joan Bruna, Dumitru Erhan, Ian J. Goodfellow, and Rob Fergus. Intriguing properties of neural networks. In Yoshua Bengio and Yann LeCun, editors, *2nd International Conference on Learning Representations, ICLR 2014, Banff, AB, Canada, April 14-16, 2014, Conference Track Proceedings*, 2014.
- [62] Florian Tramèr, Nicholas Carlini, Wieland Brendel, and Aleksander Madry. On adaptive attacks to adversarial example defenses. In Hugo Larochelle, Marc’Aurelio Ranzato, Raia Hadsell, Maria-Florina Balcan, and Hsuan-Tien Lin, editors, *Advances in Neural Information Processing Systems 33: Annual Conference on Neural Information Processing Systems 2020, NeurIPS 2020, December 6-12, 2020, virtual*, 2020.
- [63] Florian Tramèr, Fan Zhang, Ari Juels, Michael K. Reiter, and Thomas Ristenpart. Stealing machine learning models via prediction apis. In Thorsten Holz and Stefan Savage, editors, *25th USENIX Security Symposium, USENIX Security 16, Austin, TX, USA, August 10-12, 2016*, pages 601–618. USENIX Association, 2016.
- [64] Gerrit J. J. van den Burg and Christopher K. I. Williams. An evaluation of change point detection algorithms. *arXiv preprint arXiv: 2003.06222*, 2020.
- [65] Zekai Wang, Tianyu Pang, Chao Du, Min Lin, Weiwei Liu, and Shuicheng Yan. Better diffusion models further improve adversarial training. *CoRR*, abs/2302.04638, 2023.
- [66] Dongxian Wu, Yisen Wang, Shu-Tao Xia, James Bailey, and Xingjun Ma. Skip connections matter: On the transferability of adversarial examples generated with resnets. In *8th International Conference on Learning Representations, ICLR 2020, Addis Ababa, Ethiopia, April 26-30, 2020*. OpenReview.net, 2020.
- [67] Cihang Xie, Jianyu Wang, Zhishuai Zhang, Zhou Ren, and Alan L. Yuille. Mitigating adversarial effects through randomization. In *6th International Conference on Learning Representations, ICLR 2018, Vancouver, BC, Canada, April 30 - May 3, 2018, Conference Track Proceedings*. OpenReview.net, 2018.
- [68] Cihang Xie, Zhishuai Zhang, Yuyin Zhou, Song Bai, Jianyu Wang, Zhou Ren, and Alan L. Yuille. Improving transferability of adversarial examples with input diversity. In *IEEE Conference on Computer Vision and Pattern Recognition, CVPR 2019, Long Beach, CA, USA, June 16-20, 2019*, pages 2730–2739. Computer Vision Foundation / IEEE, 2019.
- [69] Heng Yin, Dawn Song, Manuel Egele, Christopher Kruegel, and Engin Kirda. Panorama: capturing system-wide information flow for malware detection and analysis. In *Proceedings of the 14th ACM conference on Computer and communications security*, pages 116–127, 2007.

## A More Theoretical Analysis

### A.1 Modeling Image Interpolation

In Section 4.3.2, we define the template matching score  $\mathcal{M}$  using Pearson correlation coefficient as follows:

$$\mathcal{M}(\delta_t, \tau) := |R(\delta_t, \tau)|, \quad (12)$$

where  $\delta_t$  is the per-query changes and  $\tau$  is the template that we extracted from the binarized power spectral density when enrolling new attacks in Section 6.

However, this definition may not cover all scenarios, such as the image line search step that interpolates between the clean image  $\mathbf{x}$  and the candidate adversarial example  $\mathbf{x}''$ . In this case, the per-query changes  $\delta$  would correlate with the clean image and the final adversarial example.

To model this procedure, we let  $\tau := \mathbf{x}'$  and follow the same definition as other pattern procedures. This way, we can characterize procedures that produce changes correlated with the adversarial example. This refers to the `IMG` procedure.

### A.2 Modeling General Line Search

Some attacks may also apply linear search over the factor  $a$  multiplied by a fixed noise  $\eta$ :

$$\begin{aligned} \mathbf{x}_{t-1} &= \mathbf{x} + a_1 \cdot \eta \\ \mathbf{x}_t &= \mathbf{x} + a_2 \cdot \eta, \end{aligned} \quad (13)$$

where the per-query change  $\delta_t$  would become noise. Instead of matching  $\delta_t$  to a pre-defined template, we match its linear relationship with the previous per-step change  $\delta_{t-1}$  using cosine similarity, written as

$$\mathcal{M}(\delta_t, \delta_{t-1}) := \text{cos-sim}(\delta_t, \delta_{t-1}) = \frac{\delta_t \cdot \delta_{t-1}}{\|\delta_t\| \|\delta_{t-1}\|}, \quad (14)$$

where both changes are flattened into vectors.

In this way, we can model the general line search procedure `LS` in the same framework as defined in Equation (5). The only exception is that the probability will now condition on two previous queries  $P(\mathbf{x}_t | \mathbf{x}_{t-1}, \mathbf{x}_{t-2})$ .

### A.3 Transforming Similarity Score to Probability

In Equation (5), we transform the above similarity score to a probability distribution by enforcing a truncated exponential distribution on  $\mathcal{M}$ , defined as

$$P(\mathbf{x}_t | \mathbf{x}_{t-1}) := c \cdot \frac{1}{|\mathbb{D}|^{1-\mathcal{M}(\delta_t, \tau)}}, \quad (15)$$

where  $c$  is the normalization constant. We now explain the intuition behind this definition step by step.

First of all, one may want to regard the similarity score  $\mathcal{M}$  as an off-the-shelf probability. However, this is not a valid probability measure because it does not sum to one over the entire input space  $\mathbb{D}$ .

The second option is dividing this score by  $|\mathbb{D}| = 256^d$  so it sums up to one and therefore becomes a valid probability distribution. However, this option would prevent the activation of pattern procedures in the

face of other noise procedures because the resulting probability will never approach 1, even with a perfect matching. The same problem applies when normalizing the score with softmax.

Finally, we enforce a truncated exponential distribution on  $\mathcal{M}$ , so its probability concentrates on a perfect matching yet decreases to zero exponentially upon a bad matching. One may derive this by following a similar idea as noise procedures, where the probability applies independently to each single pixel. That is, for a given similarity score  $\mathcal{M}$ , we assume each pixel  $\{\delta_i\}_{i=1}^d$  of  $\delta_t$  will have a probability of  $256^{\mathcal{M}}/256$ . Thus, the probability of  $\delta_t$  can be defined as

$$P(\mathbf{x}_t|\mathbf{x}_{t-1}) := \prod_{i=1}^d \Pr[\delta_i] = \frac{256^{d\mathcal{M}}}{256^d} = |\mathbb{D}|^{\mathcal{M}-1}, \quad (16)$$

which resembles Equation (15) after normalization.

#### A.4 Details of System Implementation

We summarize our algorithm for discovering procedures from a given trace  $X$  in Algorithm 1. We generally set the thresholds to  $\tau_{\text{segment}} = 500$  and  $\tau_{\text{merge}} = 250$ .

---

##### Algorithm 1 Discover Procedures

---

**Require:** The attack trace  $X = \{\mathbf{x}_i\}_{i=1}^n$ .

**Ensure:** Clusters of sub-traces  $\mathbb{X}$ , where each cluster  $\mathbb{C} \in \mathbb{X}$  contains sub-sequences from the same procedure.

```

1:  $\triangleright$  Get the power spectral density of per-query changes
2:  $\{\delta_i\}_{i=1}^{n-1} \leftarrow \{\text{FFT2}(\mathbf{x}_{i+1} - \mathbf{x}_i)\}_{i=1}^{n-1}$ 
3:  $\mathbb{X} \leftarrow \emptyset$   $\triangleright$  Initialize the set of clusters
4:  $\mathbb{C} \leftarrow \emptyset$   $\triangleright$  Initialize one cluster
5: for  $i \leftarrow 1$  to  $n - 2$  do
6:    $\mathbb{C} \leftarrow \mathbb{C} \cup \{\delta_i\}$   $\triangleright$  Procedure continues
7:   if  $\text{MSE}(\delta_i - \delta_{i+1}) > \tau_{\text{segment}}$  then
8:      $\mathbb{X} \leftarrow \mathbb{X} \cup \{\mathbb{C}\}$   $\triangleright$  Procedure completes
9:      $\mathbb{C} \leftarrow \emptyset$ 
10:  end if
11: end for
12:  $\mathbb{X} \leftarrow \mathbb{X} \cup \{\mathbb{C}\}$   $\triangleright$  The last procedure
13: for  $i \leftarrow 2$  to  $|\mathbb{X}|$  do
14:    $\{\bar{\delta}_j\}_{j=1}^i \leftarrow \sum_{\delta \in \mathbb{X}_j} \delta / |\mathbb{X}_j|$   $\triangleright$  Compute means
15:    $\mathbb{C}^* \leftarrow \arg \min_{\mathbb{C}_j \in \mathbb{X}_{1:i}} \text{MSE}(\bar{\delta}_i - \bar{\delta}_j)$   $\triangleright$  Find closest
16:   if  $\text{MSE}(\bar{\delta}_i - \bar{\delta}^*) < \tau_{\text{merge}}$  then
17:      $\mathbb{C}^* \leftarrow \mathbb{C}^* \cup \mathbb{X}_i$   $\triangleright$  Merge if close enough
18:   end if
19: end for
20: return  $\mathbb{X}$ 

```

---



## B More Experimental Details and Results

### B.1 Datasets and Models

We provide more details about the datasets and models we used for evaluation.

#### ImageNet

We randomly select 200 images of size  $224 \times 224$  from the validation split as the clean image of all attacks we consider. We use three different models, including ResNet-50, WRN-50-2, Swin-T. These models are pre-trained by TorchVision<sup>1</sup> on the ImageNet dataset, with Top-1 accuracy of 80.858%, 81.602%, and 81.474%, respectively.

#### CelebA

We randomly select 200 images and rescale the images to  $224 \times 224$  from the validation split as the clean image of all attacks. We use two models ResNet-18 and ResNet-34. These models are pre-trained on the CelebA dataset to predict the Mouth\_Slightly\_Open and the Gender attribute with accuracy 92.4% and 95.3%.

#### CIFAR10

We randomly select 500 images of size  $32 \times 32$  from the test split as the clean image of all attacks. We use two models WRN-28-10 and WRN-70-16. These models are provided by RobustBench [20] with Top-1 accuracy of 94.78% and 95.54%, respectively. In particular, the second model attains robust accuracy 84.98% under  $\ell_2$  norm perturbation  $\epsilon = 0.5$  [65].

### B.2 Attack Configurations

We use ART for the first four attacks and BBB for the last four attacks.

**HSJ [13]** This is the improved Boundary [10] attack. At each iteration, it refines the perturbation by estimating the gradient direction and using binary search to approach the decision boundary.

**GeoDA [54]** This attack is similar to HSJ [13], but leverages the geometry property of decision boundary and sub-space Gaussian noise to improve the gradient estimation.

**SignOPT [19]** This attack solves a zeroth-order optimization problem by estimating the sign of each step.

**Square [7]** This score-based attack adds squares to the image to estimate the loss.

**Boundary [10]** This is the first decision-based attack without estimating the gradients. It finds an adversarial example close to the decision boundary and iteratively refines it to mislead the model without needing access to gradients.

---

<sup>1</sup><https://pytorch.org/vision/stable/models.html>

**ECO [44]** This score-based attack optimizes adversarial perturbation by splitting the image into blocks.

**RayS [14]** This  $\ell_\infty$  decision-based attack reformulates the continuous problem of finding the closest decision boundary into a discrete problem that does not require any zeroth-order gradient estimation.

**NES [34]** This score-based attack uses natural evolution strategies to improve gradient estimation.

### B.3 Explain the Square Attack

We first outline the sketch of ART’s implementation of the Square-2 attack as follows.

```
for i in range(num_iters):
    # Do we continue?
    score = query(x_adv)
    if success(score):
        break

    # Get adv noise
    score = query(x_adv)
    noise = get_noise(score)
    x_adv_new = x_adv + noise

    # Does it improve?
    score = query(x_adv_new)
    if better(score):
        x_adv = x_adv_new
```

In the above code, we identify two cases where it might send duplicate queries to the model.

1. The first query call is only used for checking if the current adversarial example is successful. This output can be reused in the next query, where the attack attempts to get the score from the model. This duplication makes around 50% of the total queries unnecessary.
2. The last query call determines if the new candidate adversarial example obtains a lower score. If it is not better, the adversarial example will not be updated; hence the same output can be reused in the next iteration’s first query. This duplication is triggered less frequently than the previous one.

### B.4 More Visualizations

We visualize the average and 95% confidence interval of all fingerprints for each attack in Figure 11.

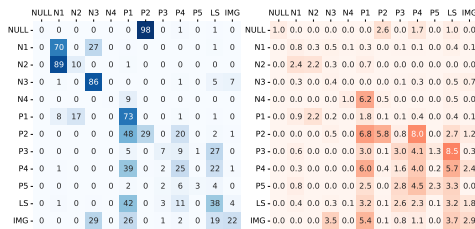
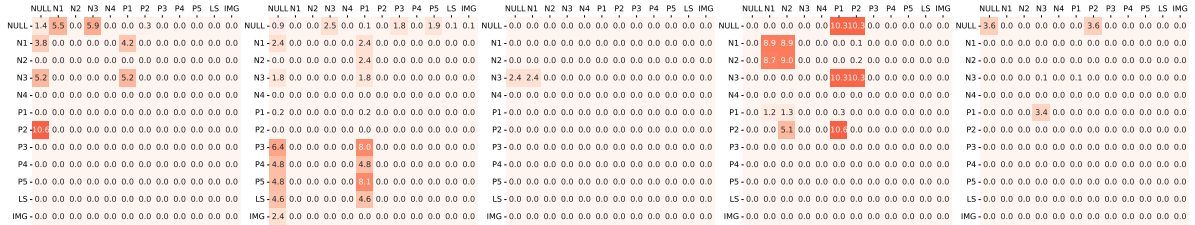
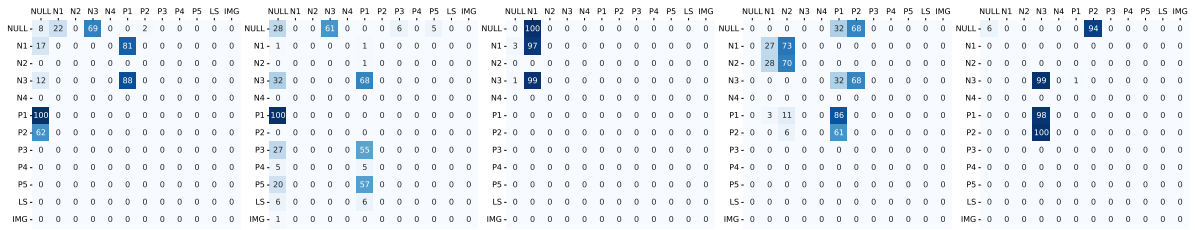
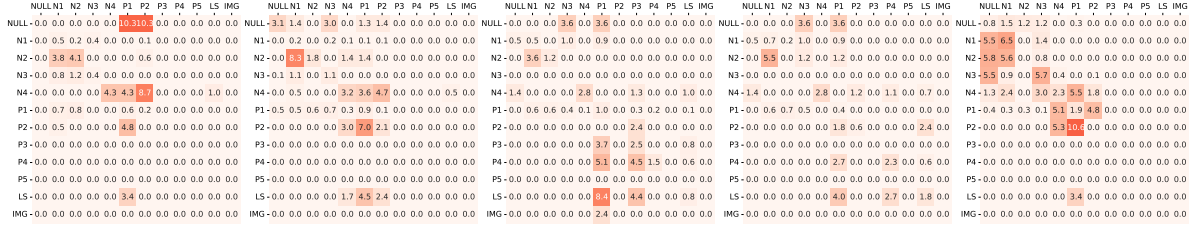
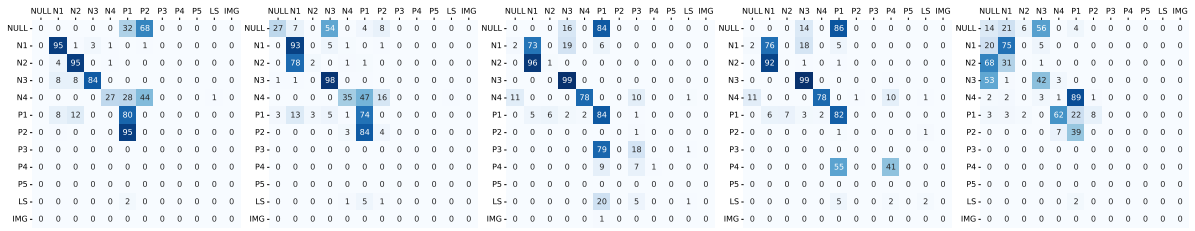


Figure 11: The average (blue) and 95% confidence interval (orange) of the fingerprints of each attack. Each fingerprint is generated from only one trace.